THEORETICAL ASPECTS OF SORPTION REFRIGERATION USING ORGANIC COMPOUNDS

by
Meihua Jin

A dissertation submitted to the University of Cape Town
in fulfillment of the requirements for the degree of
Master of Science in the Department of Mechanical Engineering

Cape Town
May 2016

Supervised
by
A/Professor George Vicatos

Contents

Declaration

I, the undersigned, hereby declare that this dissertation entitled "Theoretical aspects of sorption refrigeration using organic compounds" is my own work, and that all the sources I have used or quoted have been indicated or acknowledged by means of completed references.

Signed by candidate

15/02/2016

EBE Faculty: Assessment of Ethics in Research Projects

Any person planning to undertake research in the Faculty of Engineering and the Built Environment at the University of Cape Town is required to complete this form before collecting or analysing data. When completed it should be submitted to the supervisor (where applicable) and from there to the Head of Department. If any of the questions below have been answered YES, and the applicant is NOT a fourth year student, the Head should forward this form for approval by the Faculty EIR committee: submit to Ms Zakiya Chikte (Zakiya.chikte@uct.ac.za); New EBE Building, Ph 021 650 5739).

Please note – It is important to keep a signed copy of this form as students must include a copy of the completed form with the dissertation/thesis when it is submitted for examination.

Name of Principal Researcher/Student: Meihua Jin **Department:** Mechanical Engineering

JNXMEI001

If a Student: **Degree:** MSc **Supervisor:** A/Prof. George Vicatos

If a Research Contract indicate source of funding/sponsorship:

Research Project Title: Theoretical Aspects of Sorption Refrigeration Systems Using Organic Compounds

Overview of ethics issues in your research project

Question 1: Is there a possibility that your research could cause harm to a third party (i.e. a person not involved in your project)?	YES	NO ✓
Question 2: Is your research making use of human subjects as sources of data? If your answer is YES, please complete Addendum 2.	YES	NO ✓
Question 3: Does your research involve the participation of or provision of services to communities? If your answer is YES, please complete Addendum 3.	YES	NO ✓
Question 4: If your research is sponsored, is there any potential for conflicts of interest? If your answer is YES, please complete Addendum 4.	YES	NO ✓

If you have answered YES to any of the above questions, please append a copy of your research proposal, as well as any interview schedules or questionnaires (Addendum 1) and please complete further addenda as appropriate.

I hereby undertake to carry out my research in such a way that

- there is no application for objection to the nature or the method of research; and
- the research will not compromise staff or students or the other responsibilities of the University;
- the stated objectives will be achieved, and findings I have a high degree of validity;
- limitations and alternative interpretations will be considered;
- the findings could be subject to peer review and publicly available; and
- I will comply with the conventions of copyright and avoid any practice that would constitute plagiarism.

Signed by: Signed by candidate

Full name and signature

Principal Researcher/Student: Signed by candidate

Date: 15/02/16

This application is approved by:

Supervisor (if applicable):

HOD (or delegated nominee):
Final authority for all assessments by staff and undergraduate research.

Chair : Faculty EIR Committee
For applicants other than undergraduate students who have answered YES to any of the above questions.

Abstract

Refrigeration devices for essential food storage and preservation of medicine are among the most significant techniques developed in the past few decades. In many regions of Africa, the shortage of sustainable power sources and the abundance of solar energy make solar refrigerators a promising solution for basic refrigeration needs. Among all the solar cooling techniques, the solar sorption refrigerator is considered to be a promising alternative to the dominant vapour-compression refrigerator, which encompasses both absorption and adsorption refrigerators. It has advantages of being silent, having no compressor, lasting a long life cycle, and utilising waste heat or solar energy. In this work, the development of sorption refrigerators is outlined, and as a part of it, a theoretical diffusion absorption chiller using organic compounds is designed. The alternative working fluids used is R134a as the refrigerant, tetraethylene glycol dimethyl ether (TEG.DME) as the absorbent, and helium as the auxiliary gas. The corresponding modelling is carried out as a potential cooling system based on calculations.

Furthermore, as a second part of this work, a laboratory prototype of a solid adsorption system being developed by the "Institute of Chemical Process Engineering (ICVT)" in Stuttgart University, is studied and compared. The study focuses on adsorption properties of methanol on activated carbon in adsorption process. Adsorption equilibrium data has been measured, and a good agreement between the measured equilibrium data and theoretical Dubinin-Astakhov model has been obtained. This prediction model can now be used to provide accurate data-sets, and consequently help to optimise the adsorption performance of the cooling unit.

The results of the project lead to a two-fold conclusions with respect to the liquid-gas absorption and solid-gas adsorption systems based on laboratory-size prototypes. The derived experimental hardware and procedures of the absorption system and the experiments conducted in determining pressure/temperature relationships of the adsorption system can help to optimise proposed designs and operating conditions that will facilitate the development of a new energy-efficient cooling plant.

Nomenclature

Acronym:

AC: Activated carbon
CFC: Chlorofluorocarbon
HCFC: Hydrochlorofluorocarbon
HFC: Hydrofluorocarbon
HFO: Hydrofluoroolefin
COP: For refrigerator: The ratio of the refrigeration capacity to the power absorbed by the compressor. For heat pump: The total heat delivered to the power absorbed by the compressor.
DAR: Diffusion absorption refrigeration
DMAC: N,N-Dimethyl acetamide
DMEU: Dimethyl-Ethylene Urea
DMF: N,N-Dimethyl formamide
GHX: Gas heat exchanger
GWP: Global warming potential(A measure of how much heat a greenhouse gas traps in the atmosphere relative to carbon dioxide).
Heat Sink: A destination, to where a device provides heat energy from a source of heat (e.g. eternal temperatures). Corresponding to the low temperature heat source.
HTC: Heat transfer coefficient
MCL: N-methyl ε-caprolactam
NREL: American national renewable energy laboratory
Nu: Nusselt number
ODP: Ozone depletion potential. The potential of a substance to destroy stratospheric ozone.

PAC: Powdered activated carbon

Pr: Prandtl number

Re: Reynolds number

R134a: 1,1,1,2-tetrafluoroethane(HFC)

SCP: Specific cooling power, the ratio of cooling capacity to mass of adsorbent in the absorbers.

SEM: Scanning electron microscope

SHE: Solution heat exchanger

TEG.DME: Tetraglyme, or tetraethylene glycol dimethyl ether

TGA: Thermogravimetric analysis

VOC: Volatile organic compounds

Units and Symbols:

$\mathring{A}$**:** *Ångström*

c**:** Specific heat capacity $(kJ/kg \cdot K)$

f'**:** Circulation ratio(solution circulation rate per unit of refrigerant generated)

f**:** Darcy friction factor

k**:** Thermal conductivity $(W/m \cdot K)$

$\dot{m}$**:** mass flow rate (kg/s)

$\Delta Hvap$**:** Latent heat of vaporization (kJ)

ν**:** Momentum diffusivity (kinematic viscosity) (m^2/s)

α**:** Thermal diffusivity (m^2/s)

c**:** Specific heat $(J/kg \cdot K)$

μ**:** Dynamic viscosity $(kg/m \cdot s)$

M**:** Molecular weight of methanol (J/kg)

R**:** The universal gas constant $(J/mol/K)$

U**:** Overall heat transfer coefficient $(W/m^2 \cdot^\circ \text{C})$.

h_i/h_o**:** The individual convection heat transfer coefficient of the inside or the outside of the heat transfer wall $(W/m^2 \cdot K)$.

A_i/A_o**:** The area of the inner or outer surface of the heat transfer wall.

Subscripts:

c: Condenser
cr: Refrigerant states at the condenser
cw: Cooling water states at the condenser
e: Evaporator
er: Refrigerant states at the evaporator
ew: Cooling water states at the evaporator
pc: Pre-cooler
pcr: Refrigerant states at the pre-cooler
pcw: Cooling water states at the pre-cooler
a: Absorber
ar: Refrigerant states at the absorber
aw: Cooling water states at the absorber

Acknowledgements

I wish to express my sincere appreciation and gratitude to A/Prof. George Vicatos, who undertook to act as my supervisor. His wisdom, knowledge and philosophy to the highest standards inspired and motivated me.

Besides my supervisor, I would like to thank Mr. Hubert Tomlinson, who has played a pivotal role in this dissertation. He has far exceeded his duty as a technical advisor, helping me through the completion of the prototype.

In Germany, I acknowledge my mentor, Mr. Philipp Günther, who has shared his invaluable knowledge in the chemical process engineering field, diffusion and adsorption theories, experimental operation methods, MATLAB coding, and data calibration, etc. He was and remains my best role model for an academic, mentor, and friend.

My sincere thanks also goes to Mr. Michael Young, a loyal friend and an enthusiastic partner in this endeavour, who has shown me great passion in the HVAC industry and always acted as a co-supervisor, guiding me through the project.

I'd like to extend my profound gratitude to my friend, Dr. Chen Wei, from the department of computer science, for his help not only with computational techniques and software in general, but also in giving me invaluable support and encouragement on my way pursuing the master degree and my entire graduate career.

I thank my friend and colleague, Niran Ilangakoon, who selflessly put much effort in helping me with the final dissertation proof-reading. Many thanks for your time.

I am also very grateful to my friends Rui Zhang, Qiao Xiong, Ebrahim Osman, Naomi Li, Danny Cheung, Roberto Gomes, Louis Feng, and David Zhang. Without their on-going support, I could not have finished this dissertation and had the most glorious time of my life in this beautiful country.

Last but by far not the least, I would love to express my sincerest thanks to my parents, Wenguo Jin and Jingai Shi, who have always supported, encouraged and believed in me, in all my endeavours. This dissertation is dedicated to them.

List of Figures

List of Tables

Chapter 1

Introduction

The term sorption encompasses both absorption and adsorption processes, which is also known as thermochemical sorption or liquid sorption for absorption, and physisorption or solid sorption for adsorption, respectively. Conceptually, sorption refrigerators utilise "thermal compressors" instead of electrically-driven compressors found in conventional household refrigerators. The vapour is obtained by applying heat to a refrigerant solution or subjecting it to vacuum. The primary category of solar cooling techniques is summarised in Figure 1.1.

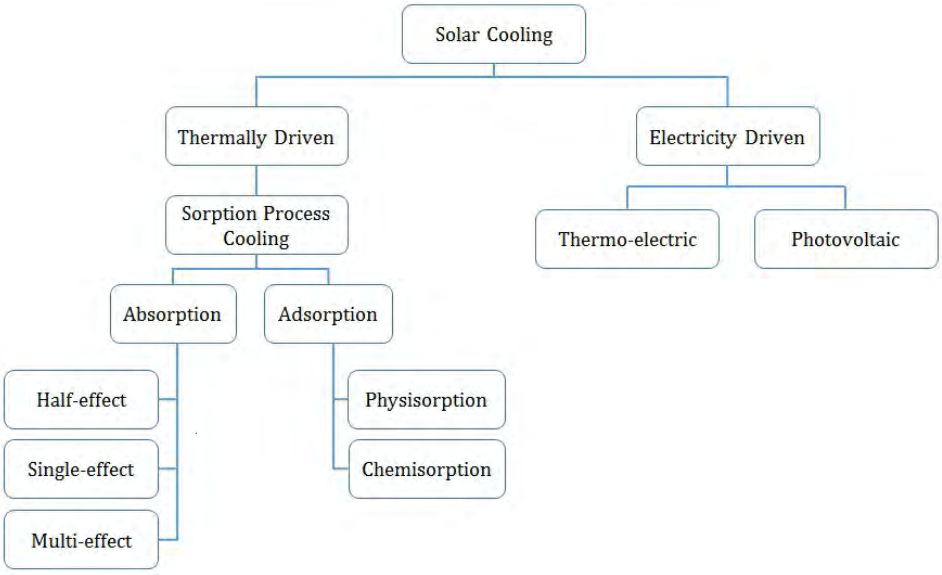

Figure 1.1: Solar-driven cooling systems category

According to the International Institute of Refrigeration, refrigeration technology and air conditioning account for approximately 15 % of the worldwide electricity consumption [60] [15]. In Mediterranean countries, solar-driven cooling systems are predicted to reduce energy costs by approximately 50 % [6].
Although this appealing concept has been studied for centuries and has become a relatively advanced technology, the lack of economic viability is the biggest hindrance to its large scale adaptation. The majority of the latest installed solar cooling systems are still prototype-based, although some manufacturers have entered the market with series production [14].

1.1 Dissertation aims and organisation

The dissertation mainly encompasses two branches of study of sorption refrigeration. It starts with a background literature survey on the classification of existing refrigerators, followed by specific study of absorption and adsorption cooling techniques, respectively.
In the absorption cooling study, the primary focus was on the macroscopic design, which aims at modelling of a three-fluid diffusion absorption refrigeration unit using organic compounds (R134a and TEG.DME). Helium was used as the third fluid instead of Hydrogen for the diffusion process.
In the adsorption cooling study, the focus was on the particle level about working pairs'(methanol and activated carbon) characteristics and thermochemical performance, which aims at theoretical modelling of an intermittent adsorption system and experimental verification of the predictive performance. Computerised control of the adsorption unit was employed, intensive pressure and temperature responses were captured and used to fit theoretical models.
Both theoretical study and experimental investigation were combined in this work for a better understanding of sorption refrigeration.

1.2 Classification and review of refrigerators

In this section, the existing literature on cold generation technologies is outlined, the result will build the accumulation of solar refrigeration know-how in our research.

1.2.1 Vapour-compression refrigerator using refrigerant of HCFCs/HFCs

Vapour-compression system, used by common household refrigerators, was first built in the late 19th century and became commonplace after 1940. The basic cooling cycle is shown in Figure 1.2.

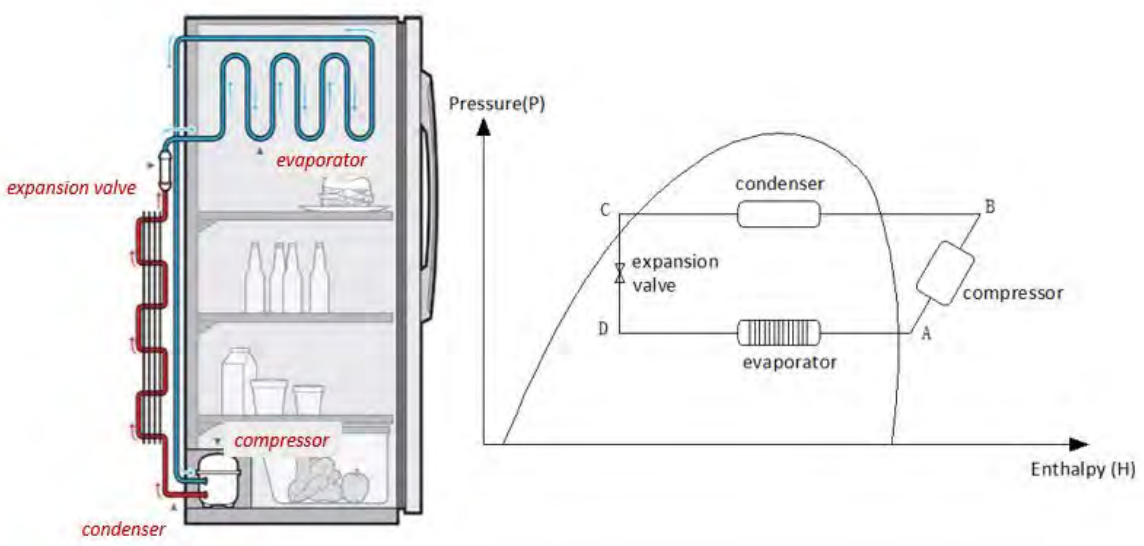

Figure 1.2: Vapour-compression refrigerator and its Pressure-Enthalpy diagram

From 1930∼1990, CFCs and HCFCs were increasingly used, such as R22, for air conditioning, and R12, for medium and high-temperature refrigeration. Following the significant damage to the environment, and the depletion of O-zone layer, the Montreal protocol was signed in 1989. CFC refrigerants were no longer available in Europe after January 1, 1995, and globally after January 1, 1996.

HCFC refrigerants like R22 have also been banned for use in new systems in Europe since January 1, 2000. HFCs were proved to be transition substances from 1990 up to the recent, among which, R134a (1.1.1.2-tetrafluoroethane) is seen to be a promising refrigerant because of its favourable solubility with some organic solvents, and a relatively smaller GWP of 1430 compared to other HFCs (such as R404a, R410a, etc.). Substances that have even lower GWP, such as HFO-1234yf are under-way.

Table 1.1: Refrigerant representatives of CFCs, HFCs and HFOs [28]

Refrigerant	R-12 Dichlorodifluoromethane	R134a Tetrafluoroethane	R1234-yf Tetrafluoroprop
ODP	0.82	0	0
GWP	10900	1430	4
STATUS	No manufacture universally after-1996-01-01	2030 in developed countries 2040 in developing countries	Potential replacement for R134a

1.2.2 Vapour absorption refrigerator using working pair of $NH_3\,(R717)$ and H_2O

Ammonia system has its advantages of good solubility and high latent heat and disadvantages of toxicity and comparatively low COP. An evolution in the early age of refrigeration development was with the launch of the first absorption refrigerator introduced by Ferdinand Carre in 1859 using NH_3 and H_2O. The working pair is then in latter days, seen as the most common commercially working agent.

The first diffusion absorption refrigeration system was invented by two students, Baltzar von Platen and Munters. It went into production in 1923 by Electrolux [18] as illustrated in Figure 1.3. This system forms the basis of the design employed in this project.

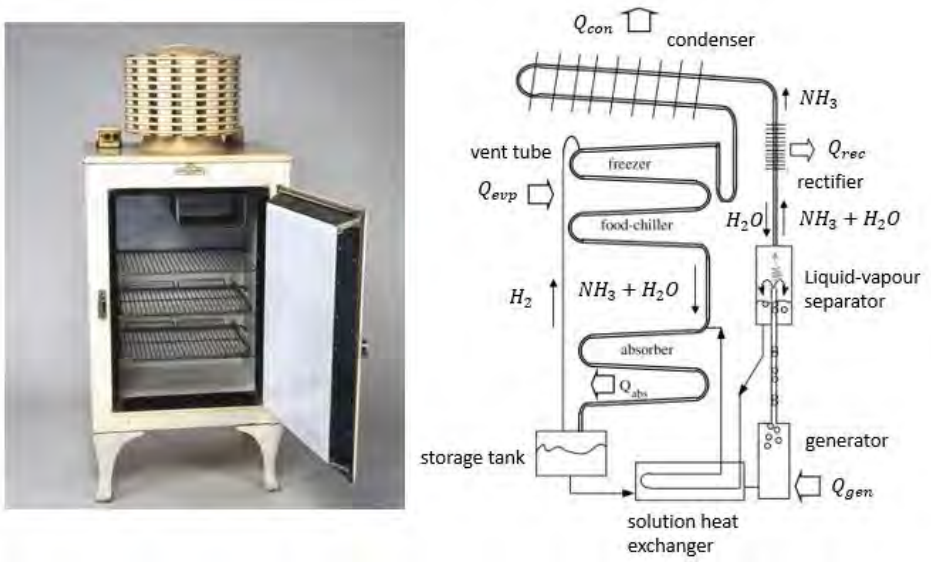

Figure 1.3: The first version of diffusion absorption refrigerator(DAR) by Baltzar von Platen and Munters

1.2.3 Vapour absorption Einstein refrigerator

At around the same time that Von Platen and Munters were developing the ammonia refrigerator, Albert Einstein and his colleague Leo Szilard jointly invented another version of the diffusion absorption refrigerator. The invention was motivated by a tragic death of an entire family in Berlin due to the leakage of toxic refrigerants (the commonly used methyl chloride, ammonia or sulphur dioxide [12]). The more stable thermally-driven refrigerator [1] avoided abrasion, which was a common problem in mechanical systems. It used pressurised ammonia as a pressure equalizing fluid instead of inert gas, butane as the refrigerant, and water as the absorption liquid. An illustration of this system is shown in Figure 1.4.

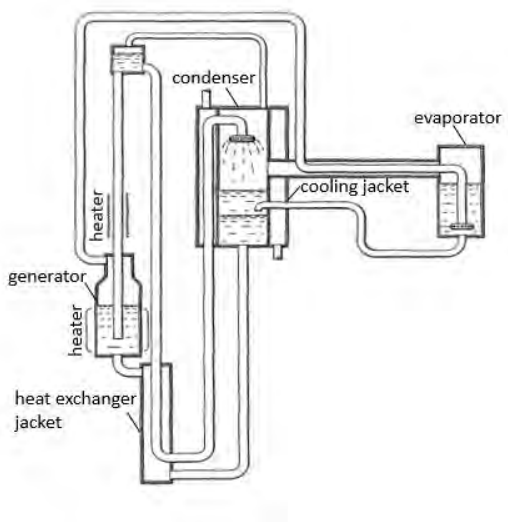

Figure 1.4: Einstein refrigerator

The changes of the system configurations and working fluids improved COP to 0.25 in comparison with that of $0.15 \leq COP \leq 0.2$ [36] achieved by the Platen and Munters cycle. As a result of low COPs and the advent of the electric refrigerator, these designs soon faded out after 1930. However, many variations based on the original DAR cycle were developed and were mainly used for camping and caravans.

1.2.4 Vapour absorption refrigerator using working pair of H_2O and $LiBr$

The first single-effect H_2O-$LiBr$ absorption refrigerator was developed by Carrier company in 1945. The system was not able to work efficiently at generation temperatures lower than 90 °C [26], and with water as refrigerant, the minimum temperature of 0 °C is used more in the air-conditioning industry. Disadvantages include the ease of crystallisation, and the occurrence of severe corrosion problems at generation temperatures higher than 200 °C. It operates below atmospheric pressure, at around 0.008 bar in the evaporator, with a corresponding vaporization temperature of approximately 3 °C [43].

1.2.5 Vapour absorption refrigerator using working pair of organic compounds

As very few single substances are suitable to be used as refrigerants/absorbents, extensive research has been carried out on the use of blends of existing substances.
Since the late 1950s, some pioneering studies on the use of fluoroalkane refrigerants with organic absorbents were carried out to investigate new refrigerant/absorbent pairs for the vapour-absorption cycle.
R134a as an alternative to CFCs in a single-stage absorption system is evaluated combined with DMAC, and the COP is varied from 0.35 to 0.46 with different evaporating and condensing temperatures [5]. The COP of R-134a/DMF (dimethyl formamide) pair is found to be 0.473 [62]. Organic absorbents like MCL (N-methyl ε-caprolactam), DMEU and TEG.DME were investigated by I Borde et al. in 1994 [9]. The values of the COP for the three combinations were similar (DMEU-0.49, MCL-0.47, and TEG.DME-0.46), but the R134a-TEG.DME system showed the best performance with lower circulation ratios, which motivated the implementation of our design with this working pair.
The literature states that there are almost 40 refrigerant compounds and 200 absorbent compounds available [31]. Table 1.2 presents some other working combinations.

1.2.6 Solid-gas type adsorption refrigerator

The adsorption process differs from the absorption process in that absorption is a volumetric phenomenon, whereas adsorption is a surface phenomenon. The technologies for refrigeration

Table 1.2: Some working combination for three-fluid single pressure absorption refrigerator

	Auxiliary Gas	Refrigerant	Absorbent
1	carbon dioxide	anodynon	water
2	NH_3	3-methyl pentane	water
3	NH_3	butane	water
4	NH_3	butane	ethylene glycol
5	methyl-amine	3-methyl pentane	ethylene glycol
6	ethyne	sulphur dioxide	acetone
7	NH_3	methyl bromide	water

purposes are rather recent. Some former intermittent cycle solar adsorption prototypes summarised by Fernandes et al. [17] were referenced. These gave rise to prototypes using the four dominated working pairs presented in Table 1.3.

Table 1.3: Common working pairs for adsorption refrigeration

Adsorbate-Adsorbent	Advantages	Disadvantages	COP
Methanol-AC [3] [20] [4] [13]	high latent heat of vaporization low adsorption heat large sorption capacity	unsuitable for heat source temperatures higher than 120 °C	0.1-0.5
Ammonia-AC [49] [45] [48] [33]	high latent heat of vaporization	toxicity and pungent smells low sorption capacity incompatible with copper	0.1-0.8
Water-Zeolite [26] [10] [4]	high latent heat of vaporization; suitable for the re-utilisation of high-temperature exhaust gas	unsuitable for applications below 0 °C high desorption temperature low heat conductivity	0.1-0.6
Water-Silica gel [38] [56] [53]	high latent heat of vaporization low adsorption heat	unsuitable for applications below 0 °C sensitive to the leakage risk	0.16-0.6

The ammonia and methanol refrigerants are the most commonly paired with activated carbon. The former is more suitable than the methanol-AC pair in case of the heat sources are higher than 200 °C [54] [29]; zeolites are hydrated aluminosilicates having porosity of 45 %∼50 % [42]. Natural zeolites have been widely used as adsorbents in separation and purification processes in the past decades; silica gel ($SiO_2 \cdot xH_2O$) is prepared from pure silica and retains chemically bonded traces of water (about 5 %). If it is overheated and loses this water, its adsorption capacity is lost, and hence, it is generally used in air conditioning. Among these alternative agents, Methanol-AC is one of the most promising working pairs in

practical systems [52] [48]. It has large adsorption quantity, low adsorption heat(1800∼2000 kJ/K) [55], and low desorption temperature of about 100 °C, which is within a suitable range for using solar energy and waste heat.

An adsorption ice maker using methanol and activated carbon was built to produce ice of about 4∼5 kg/d at an evaporator temperature of about -6 °C, and could achieve solar refrigeration COP of about 0.1∼0.12 [27]. Much achievement was obtained on the methanol-AC systems, especially at Shanghai Jiao Tong University. A prototype using the methanol-AC pair was developed and tested, producing ice of 14 kg/d in 1998 [57]. The behaviour of a continuous heat regenerative adsorption refrigeration/heat pump system employing methanol-AC pair [59] was studied, and a mathematical models to simulate the system was presented. A recent achievement by the team further realised a production of 2.6 kg ice per day per kg AC with a heat source temperature of 100 °C, and a COP of 0.13 [58]. Other than these, a recent prototype was designed with the purpose of vaccine storage by Giulio Santori et al. in 2013 (Figure 1.5). The machine operates with a 24h intermittent cycle and can produce up to 5 kg of ice per day with a solar COP of 0.08. All these confirm the possibility to employ this technology for vaccines or food conservation in remote areas.

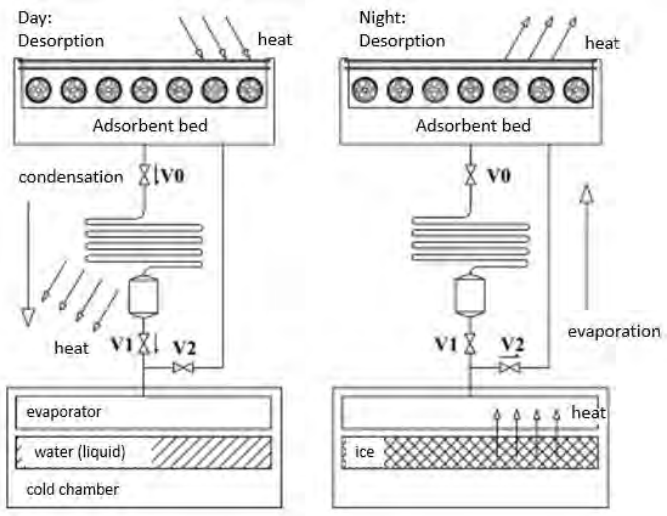

Figure 1.5: Operational phases of an intermittent solar adsorption ice maker by Giulio et al. [40]

Chapter 2

Absorption Cooling Study

2.1 Principle and Design

A solar absorption refrigerator is a device that utilises the phase-change of the refrigerant, which can be obtained by changing system temperatures and pressures, to generate an endothermic and exothermic process. Current absorption technology can provide various absorption machines with COPs ranging from 0.3 to 1.2 [22].

Conventional refrigeration systems (two-fluid design) are dual-pressure cycles where the saturation temperature difference is produced by a system pressure difference between the condenser and evaporator. However, three-fluid single-pressure diffusion absorption refrigeration (DAR) maintains a single pressure, and requires no mechanical or electrical energy, thus making it more economically viable due to fewer construction complications. Table 2.1 presents the comparison between single-pressure and dual-pressure systems.

Table 2.1: Comparison of two-fluid and three-fluid absorption systems

Criteria	Two-fluid	Three-fluid
Mechanic component	pump and expansion valve	none
Driving force	heat and electricity	heat only
Moving components	pump and valves	none
Maintenance	yes	no
Fatigue crack	likely (pressure change)	unlikely (constant pressure)

Table 2.2: Properties of the working fluids

	R134a (CH_2FCF_3)	TEG.DME ($C_{10}H_{22}O_5$)
Chemical structure	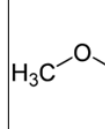	
Boiling point (atmospheric pressure)	−26.3 °C	275 °C
Critical temperature	122 °C	NA
Molar mass	102.03 g/mol	222.28 g/mol
Density	0.00425 g/ml, gas	1.009 g/mL, liquid
Solubility in water	miscible	≈0.15 % at room temperature

The following section presents the design of the 100 W solar-powered single-pressure absorption refrigeration prototype that was developed in this project. It uses R134a as the refrigerant, TEG.DME as the absorbent, and helium as the auxiliary gas. Additionally, it requires no pump for operation. The thermophysical properties of the main working fluids are as Table 2.2.

The third fluid must be chosen so as to be non-reactive to R134a, and insoluble in TEG.DME. Hydrogen is the most commonly used inert gas; other possible substitutes include Neon and Argon [39]. Helium was proposed by former researchers as the most ideal one [34].

Work done by Zohar et al. showed that the COP of an ammonia-water DAR unit working with helium was higher by up to 40 % compared to a system using hydrogen [63].

The preliminary configuration is borrowed from the first diffusion-absorption refrigeration system introduced in Sweden aforementioned [18], and the prototype built by Rodríguez-Munoz [39]. They use a non-condensable inert “expansion process” and realise a single-pressure process. The flow diagram in Figure 2.1 illustrates this model.

The cooling unit consists of the following components:

- **Boiler/Generator**

  Conventional absorption refrigerators have shown disadvantage on cost efficiency,

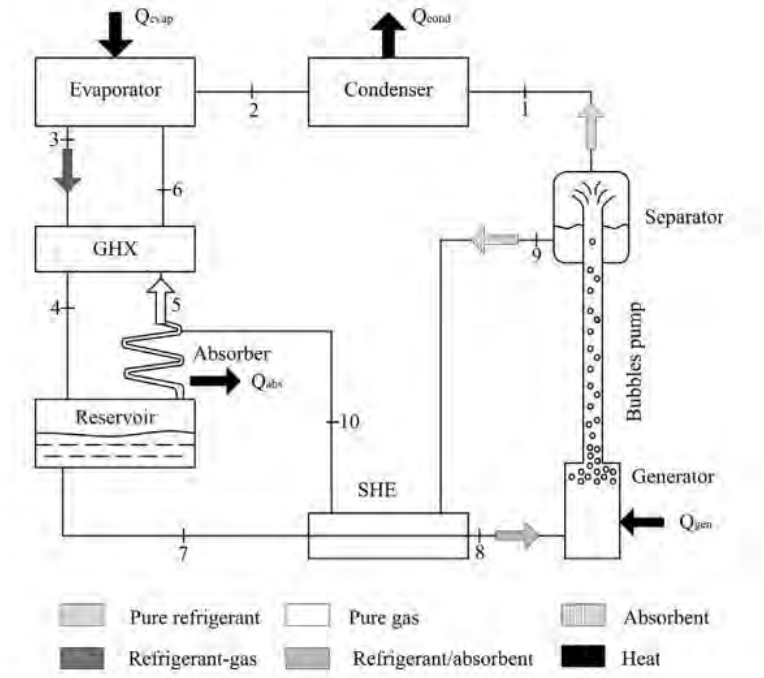

Figure 2.1: Schematic layout for a diffusion-absorption system [39]

circulation pumps alone tend to inhibit wider application, especially for those small-scale machines, hence any improvement that would alleviate the need for electrically-powered pumps would be of a beneficial.

A heat-driven bubble pump was employed in the single-effect absorption system. The mechanism moves the fluid through the cycle against flow friction and gravity. When heat is introduced to the boiler (an electrical heating element was used instead of solar heated source to simplify commissioning), bubbles of R134a gas are produced from the strong solution. The bubbles rise and pump the solution through the lift tube. The resulting weak solution then flows back in to the absorber from the separator while the R134a vapour goes to the condenser [41] [8].

For this configuration, most manufacturers used to consider multiple lift-tube bubble pumps instead of single lift-tube ones to increase its refrigeration capacity by increasing volumetric flow. However, Vicatos [50], concluded that the bubble pump with multiple tubes can increase the fluid flux but also depends strongly on the amount of heat being provided.

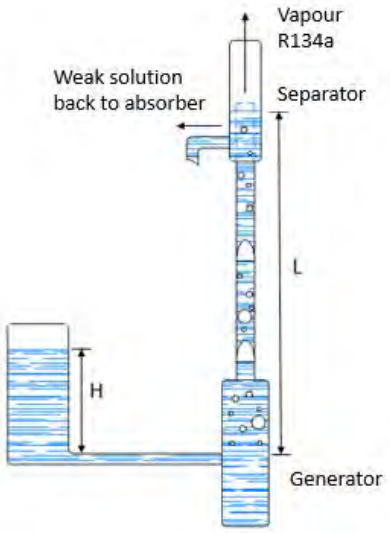

Figure 2.2: Configuration of bubble pump generator

- **Separator:**
  As illustrated in Figure 2.3, the R134a vapour and the bubbling absorbent are separated at this component.

- **Condenser and evaporator:**
  A condenser, as well as a evaporator, is typically a double pipe, counter-flow heat exchanger. The configuration has proven to be easier to construct in comparison to shell-and tube and plate-and-frame heat exchangers.

- **Pre-cooler:**
  A pre-cooler is usually used between the condenser and the evaporator to drop the refrigerant temperature from the condensate temperature to a reasonable choice before entering the evaporator. The refrigerator built by L.Filipe Mendes and M. Collares-Pereira realised a 10 % increase in COP with a 0.85 efficiency pre-cooler [32]. The use of a condensate pre-cooler in S. Arivazhagan's research [5] on R134a–DMAC also resulted in an improvement of 5 %∼15 % in the COP.

- **Generator:**
  A diagrammatic approach that was given from Vicatos [51] in an ammonia system

was used to determine the conditions in the generator. Heat supplied to the generator raises the temperature of the non-equilibrium liquor from the heat exchanger to its saturation condition. Extra heat supplied to the generator will liberate R134a and increase the saturation temperature of the solution.

- **Absorber:**
  The main purpose of the absorber is to absorb all the R134a vapour coming from the evaporator into the TEG.DME, and to separate the inert gas from the R134a vapour in the process. The weak solution (TEG.DME) coming from the solution heat exchanger enters the inner pipe of the absorber, while cold water counter flows at the annular space.

- **Solution Tank:**
  The level of the fluid in the solution tank is the same level as the solution in the boiler. It is equipped with a glass window to visually monitor the level of the solution both in the solution tank and in the generator/boiler.

- **Solution Heat Exchanger:**
  As depicted in Figure 2.3, the weak solution (TEG.DME) flowing into the inner pipe is the hot fluid and the strong solution (R134+TEG.DME) in the annulus is the cold fluid. The heat exchanger results in a reduction in both the heat supplied to the generator and in the cooling required by the absorber.

The cycle is as follows (reference to Figure 2.3):
The strong solution is heated by the heat source and produces high-pressure saturated refrigerant vapour. The vapour escapes through the lift-tube and the separator, and flows to the inner pipe of the condenser through the inverted “U” tube. Meanwhile, the separated hot weak solution flows to the absorber by gravity (hydraulic potential difference), through the inner pipe of the heat exchanger, entering the solution tank.
The liquid refrigerant passes through the pre-cooler to the evaporator and evaporates by absorbing surrounding heat at low pressure (its partial pressure).
The low-pressure vapour passes through the pre-cooler in a counter-flow direction to the liquid refrigerant from the condenser, and is entrapped by the absorbent in the absorber, liberating the inert gas, which will be free to return to the evaporator. The heat released by the absorption process will be taken away by cooling water (counter flow through the outer

tube of the absorber).
The strong solution is collected in the solution tank and flows to the generator (boiler) by gravity. The solution is then re-heated and the process is repeated.
The system remains at constant pressure by partial pressure regulation of the third fluid, which predetermines the saturation temperature of the refrigerant, and expedites the evaporation process in the evaporator. A pressure equalising tube is fitted between the condenser and the solution tank. In comparison to the vapour-compression refrigeration, the absorber, SHE, and the generator are collectively equivalent to a compressor. Further theories can be found in Waterman Gore's literature [47].

2.2 Theoretical Model

An absorption refrigeration system is based on the working fluid's characteristics, including mass and heat transfer, and chemical compositions. In order to size and build a working model, the following assumption were made:

- Steady state flow
- Kinetic and potential energy change are negligible
- The specific heat of a fluid is constant
- Axial heat conduction along the tube is negligible
- The outer surface of the heat exchangers are perfectly insulated
- Laminar flow regime expected
- Thin walled pipe neglect the conduction rate through the pipe
- Overall heat transfer coefficient based on the outside area of the inner pipe
- Average temperature used to evaluate other fluid properties

With the objective of a 100 W three-fluid DAR system in mind, the unit was designed with the assumption of a 40 °C condensing temperature, a 15 °C pre-cooler temperature, and a -5 °C evaporating temperature. From the condenser condition and the properties of saturated R-134a, the overall system pressure is 10 bar [11]. At the evaporator temperature

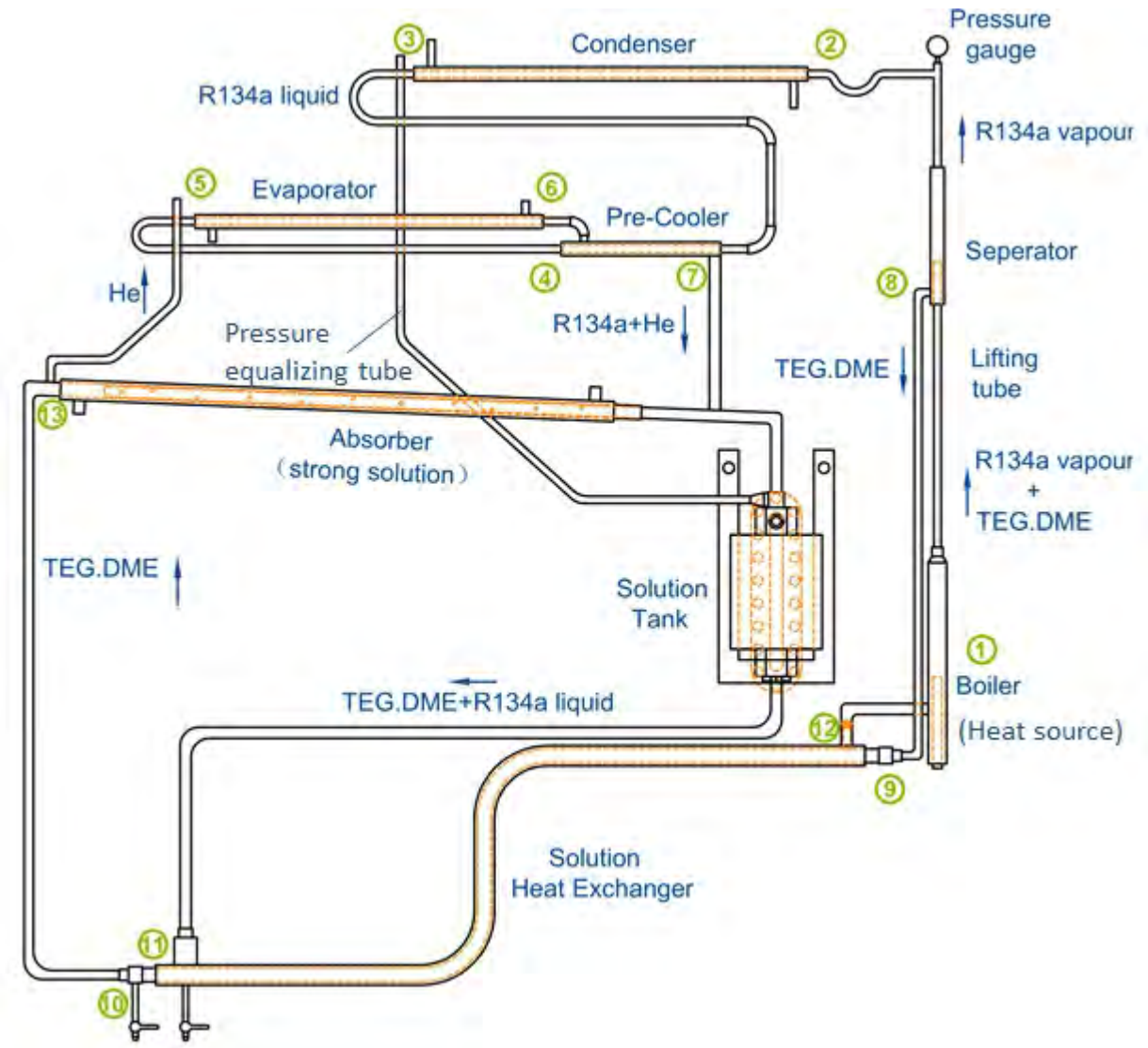

Figure 2.3: Schematic diagram for absorption refrigeration prototype

of -5 °C, the saturation pressure of R134a liquid is supposed to be roughly 2.5 bar [11]. In order to establish a uniform pressure in the system, and yet to maintain the pressure difference between the condensing and evaporating pressures, a third fluid (Helium) was added. This would enable the refrigerant to evaporate at its partial pressure in the evaporator. The value of this partial pressure was identified from Dalton's law as 7.5 bar according to:

$$P_{total} = P_{He} + P_{R134a} \tag{2.1}$$

The basic design parameters are summarised in Table 2.3.

Table 2.3: Prototype basic design parameters

Working Fluid	Generator	Type	Tubing Material	Assumed Parameter
R134a	Vapour-driven	100 W		Condenser Temp. T_c=40 °C
TEG.DME	"Pump"	Three-fluid	Copper	Pre-cooler Temp.T_{pc}=15 °C
Helium		DAR		Evaporator Temp.T_e=-5 °C

The enthalpy values are shown in Table 2.4 from the p-h diagram in Appendix E. The section below presents a part of the design calculations, details of which can be found in Appendix C. The subscript numbers correspond to the numbers shown in Figure 2.3.

- **Evaporator**

  The basic parameters and values, presented in Table2.5, are taken from the properties tables ([11] and Appendix D).

  1)Confirm the mass flow rate

  Assuming steady flow and negligible changes in kinetic and potential energies, each component has one inlet and one outlet. Thus the first law is applied for each device as:

  $$\dot{Q} = \dot{W} + \dot{m}_r(h_{out} - h_i) \tag{2.2}$$

  Since there is no work in the evaporator, we can find the heat removed from the

Table 2.4: Enthalpy values at the main points

State point enthalpy	Refrigerant conditions	Temperature (°C)	Enthalpy (kJ/kg)
h_2	superheated vapour at the inlet of the condenser	90	375
h_{st}	saturated vapour state at the condenser	40	322
h_3	de-superheated at the outlet of the condenser	40	158
$h_4 = h_5$	saturated liquid at the inlet of the evaporator	15	123
h_6	saturated vapour at the outlet of evaporator	-5	298

Table 2.5: Calculation parameters for the evaporator

Refrigerant	Temperature (°C)	$\overline{\dot{m}}\,(kg/s)$	$\overline{\mu}\,(kg/ms)$	$\overline{Pr}$	$\overline{k}\,(W/mK)$	Pipe Size(mm)
R134a	-5 (saturated liquid)	0.00057	2.947×10^{-4}	4.36	0.0968	$D_{ei} = 9.53, Th_{ei} = 0.57$
Water	13 (mean)	0.00239	1.21×10^{-3}	4.36	0.585	$D_{eo} = 15.88$,$Th_{eo} = 0.71$

refrigerated space (the evaporator) as follows:

$$\dot{Q} = \dot{m}_r(h_{out} - h_i) \tag{2.3}$$

Therefore,

$$\dot{m}_r = \frac{\dot{Q}}{\Delta h_e} \tag{2.4}$$

From $\Delta h_e = h_6 - h_5 = 175\,kJ/kg$,

$$\therefore \dot{m}_r = \frac{R_c}{Q_e} = \frac{100\,W}{17500\,J/kg} = 0.00057\,kg/s$$

As the amount of heat lost by the refrigerant equals to the amount of heat gained by the water, we can have $\dot{m}_w$ from the heat transfer formula below:

$$\Delta Q = \dot{m}_w C \Delta T \tag{2.5}$$

Where,

C = the specific heat, which for water is 4.189 $kJ/kg \cdot K$,

ΔT = the temperature difference between the water inlet and outlet temperatures. The value of the inlet water temperature is estimated as 18 °C and ΔT_w is 10 °C.

2) Calculate the Reynolds number

From the equation:

$$Re = \frac{4\dot{m}}{\pi D_h \mu} \tag{2.6}$$

Where

D_h = the inside hydraulic diameter of the pipe,

μ = dynamic viscosity of the liquid which can be found in Appendix D.

And confirmed that both the refrigerant and the coolant flows are laminar.

3) Estimate overall heat transfer coefficient

From the equation:

$$\overline{Nu} = \frac{\overline{h_i} D_h}{k} \tag{2.7}$$

We got:

$$\overline{h_i} = \frac{\overline{Nu} k}{D_h} \tag{2.8}$$

And as Nusselt number is a constant of 4.36 throughout the fully developed region [37].
Thermal conductivity values can be found from Appendix D.
From the total thermal resistance equation:

$$R = \frac{1}{h_i A_i} + \frac{\ln \frac{D_o}{D_i}}{2\pi k L} + \frac{1}{h_o A_o} \tag{2.9}$$

For the pipes with thin wall and high thermal conductivity material, it is estimated that:

$$UA = \frac{1}{R} \approx \frac{1}{h_i} + \frac{1}{h_o} \tag{2.10}$$

4) Confirm the length
The heat transfer rate across a heat exchanger is usually expressed in the form:

$$\dot{Q} = UA\Delta T_{lm} \tag{2.11}$$

Where
$\dot{Q}$ = heat transfer rate,
U = overall heat transfer coefficient,
A= heat transfer surface area,
ΔT_{lm}= logarithmic mean temperature difference.

$$\Delta T_{lm} = \frac{\Delta T_1 - \Delta T_2}{\ln \frac{\Delta T_1}{\Delta T_2}} \tag{2.12}$$

Also,

$$A = \pi D L \tag{2.13}$$

Therefore, the equation below is used for the confirmation of the length:

$$L = \frac{Q}{U\pi D\Delta T} \tag{2.14}$$

- **Condenser**

  Similar steps were taken for the calculation of the condenser, while it needs to be separated as one part from the superheated vapour state to the saturated vapour state, and the other part from the saturated vapour state to the saturated liquid state.
  As for the first part, turbulent flow is involved, and the following equation is used for calculation of Prandtl number:

$$Pr = \frac{\nu}{\alpha} = \frac{C\mu}{k} \tag{2.15}$$

  Where
  ν = momentum diffusivity (kinematic viscosity) (m^2/s),
  α = thermal diffusivity (m^2/s),
  μ = dynamic viscosity $(kg/m \cdot s)$,
  k = thermal conductivity $(W/m \cdot K)$,
  c = specific heat $(J/kg \cdot K)$.
  And for turbulent flow, Gnielinski correlation is used for Nusselt number for $0.5 \leq Pr \leq 2000$, and $3000 \leq Re \leq 5 \times 10^6$.

$$\overline{N}u = \frac{(\frac{f}{8})(Re - 1000)Pr}{1 + 12.7(\frac{f}{8})^{1/2}(Pr^{2/3} - 1)} \tag{2.16}$$

  Where friction factor f follows the equation:

$$f = (0.790 \ln Re - 1.64)^{-2}, 3000 \leq Re \leq 5 \times 10^6 \tag{2.17}$$

  And with similar calculation steps for the overall heat transfer coefficient and the logarithmic mean temperature difference, the length of the condenser can be confirmed.

Other values confirmed by the calculation (Appendix C) are presented in Table 2.6.

Table 2.6: Components dimensions of the prototype

Component	Lengths (mm)	Diameters (mm)
condenser	456	$D_o = 15.88$, $D_i = 9.53$
pre-cooler	174	$D_o = 15.88$, $D_i = 9.53$
evaporator	369	$D_o = 15.88$, $D_i = 9.53$
absorber	618	$D_o = 22.23$, $D_i = 15.88$
solution heat exchanger	629	$D_o = 19.5$, $D_i = 12.7$
generator	220	$D_o = 22.23$

2.3 Construction and Testing of the Prototype

2.3.1 Experimental Preparation

A prototype was constructed in view of obtaining a clearer concept of absorption refrigeration using organic compounds. The final experimental prototype presented in Figure 2.4 is built to comply with the analyses and calculations performed in the previous section. A heating element was used instead of a solar heater in order to use the unit during laboratory testing. A pressure gauge, and thermocouples were installed for experimental data capture.

- **Material**

  Given the working fluids, evaporating temperature and refrigeration capacity, copper is used as common material in refrigeration industry due to its high thermal conductivity, recyclability, and water resistance. It is also a highly versatile material to be used for design applications due to the availability of a variety of fittings in a wide range of diameters.

- **Hermeticity**

  Hermeticity is critical as not only externally, good gas tightness for the unit allows working fluids be filled smoothly, but also avoid leakage internally, which directly determine if the experiments can be conducted in safe. It was reported by Siemens [30] that approximately 3,000 tonnes of refrigerant p.a. of leakage occurs in Europe, and 10 % is lost during the transport, dispensing and filling processes.

  With the ease of assembly and maintenance in mind, the device was initially designed with different parts, connected as shown in Figure 2.5. However, with threaded connections and a pressurised working environment, the issue of leakage was encountered

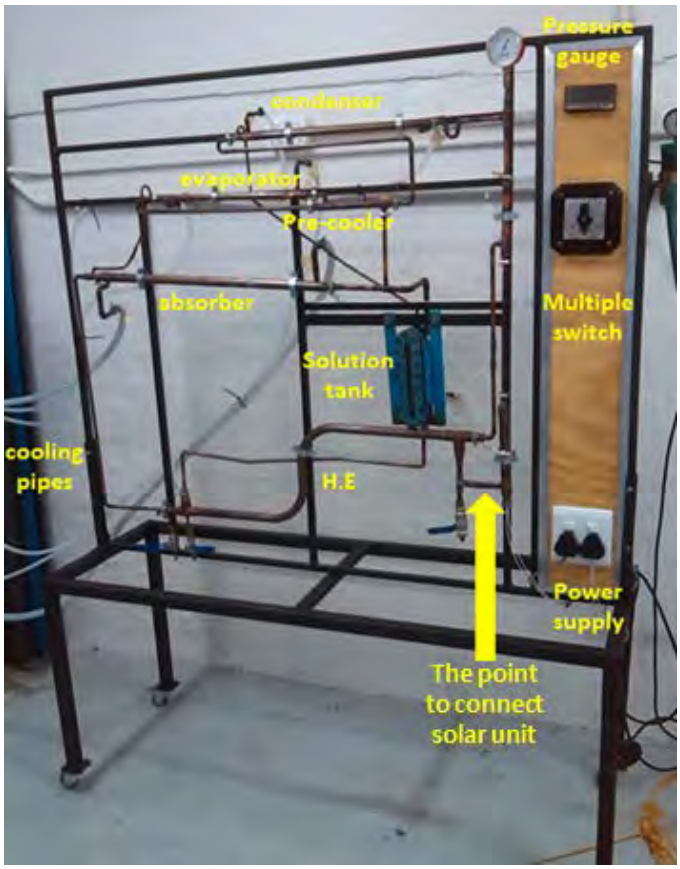

Figure 2.4: 100 W diffusion absorption refrigerator prototype using an electrical heating element as heating source. The yellow arrow indicates the position of the solar heater when the unit will be connected to use solar energy.

and fixed.

To guarantee the hermeticity and the pressure-bearing capacity of the whole system, the rig was eventually adjusted and all components were connected by welded tubes as a whole instead of threaded connections. Further, testing and pressure-verification were done by the company of "AVcape". The pressure was verified to be maintained at 20 bar for 20 minutes (Appendix B), which was a prerequisite for the experiments outlined in the following section.

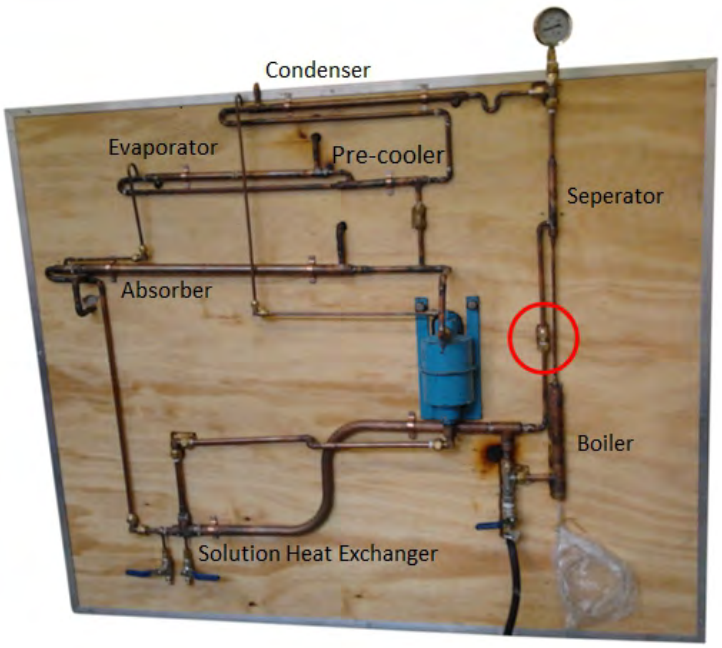

Figure 2.5: Preliminary non-integrated as-built of 100 W diffusion absorption refrigerator

- **Valve Connection**

  For the employment of valves, connections as shown in Figure 2.6 were used.

- **Instrumentation**

  Figure 2.3 shows where such measurements should be placed on our cooling system. Upgrade automatic controls can be developed further to provide accurate and flexible operation.

  Plant log sheet were kept containing information on recording day to day operation. These logs allow performance to be assessed.

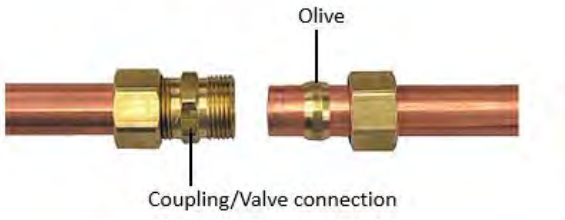

Figure 2.6: Copper pipe connection with olive

Table 2.7: Log sheet

Physical Quantity	Recording Data	Testing Point	Measuring Apparatus
Inlet/Outlet Cooling Water Temp	t_{in}, t_{out} (°C)	Inlet and Outlet of Piping	Temp. Gauge
Pressure	\	\	Pressure Gauge
Cooling Water Flow	$G\,(m^3/h)$	Piping	Flow Meter
Power Consumption	$W\,(kw)$	Switch Box	Electrodynamometer

2.3.2 Experimental Procedure

1. Draw vacuum from the system.
   Draw vacuum from from the system using a high vacuum pump, which can allow the working fluids fill into the system by pressure difference, and meanwhile provides a suitable operation environment of thoroughly dry and free of non-condensables.

2. Charge the absorbent.
   The TEG.DEM was charged into the system. The glass tube on the solution tank was used to monitor the liquid level and ensure the liquid level is just above the bubble pump.

3. Charge R134a gas into the system.
   The pressurised R134a bottle was connected to the valve. The right amount of R134a is determined by the pressure gauge.

4. Charge helium into the system.

5. Open cooling water valves to begin the cooling cycle.

6. Heating via heat element (to substitute solar unit temporally).

7. Record data every 5 minutes.

8. Stop operation by stop heat providing, and shutting down water valves.

2.3.3 Analysis of experimental failure

Experiment is the most efficient and visible way to verify a mechanism design. It is not only to have a better understanding of the operation but also to give suggestions for retrofit and reference for other similar designs.

Ideally, the prototype is supposed to perform circuit and function refrigeration. However, with the experiments carrying forward, series of concerns were met inevitably, like the heated vapour can be only lifted up to roughly 250 mm and stopped at the separator region; Or no bubbling in the boiler after several times of running. The discussion below is going to present these on-site malfunctions, retrofit was carried out using the procedure detail in the following. Some of the anomalies can be commonly confronted in experimental processes for similar designs.

- **Failure Cause 1: Circulate Malfunction**

  It was observed that heated vapour was only lifted up to separator region and no temperature increase was detected after the separator.

  Due to the small size of piping, welding block was firstly taken into consideration, while the conjecture can be directly disproved given there is always legible readings shown on the pressure gauge.

  A design defect is another possibility of the system that can lead the R134a gas to go down to the inner pipe of heat exchange instead of being lifted up by the bubbling absorbent, which can also explain the phenomenon of the rising fluid level in solution tank, which can be seen from the glass window. A steel ball then added as shown in the Figure 2.7 function as a one-way valve to avoid return of the fluid to the solution heat exchanger.

- **Failure Cause 2: Improper Inert Gas**

  To test if it was the problem from helium, we first released gas till the system reached 0 bar gauge pressure. The boiler temperature was adjusted to 80 °C by controlling the electric tension of a variable transformer. Phenomena showed the working fluid began to boil at the temperature around 40 °C and no noticeable temperature increase after the separator still. The failure conjecture was at this moment disproved.

  However, it should be pointed out that the superiority of helium was mostly examined by researchers on aqua-ammonia systems [23] [34] [24] [63]. Zohar's numerical

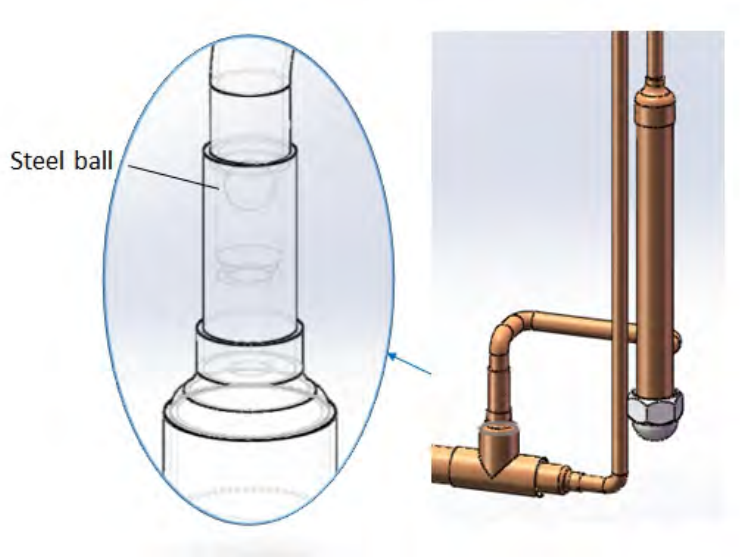

Figure 2.7: Perspective of "one-way" connection between boiler and heat exchanger

investigation (Figure 2.8) elucidates an evidently better performance by using helium as the inert gas at different experimental conditions.

Thermodynamically, helium has a smaller heat capacity than hydrogen, i.e. more heat can be absorbed by the evaporating refrigerant instead of heating of the inert gas. Consequently, more heat is absorbed from the cooling chamber, thus increasing the COP.

However, the friction losses for helium may be higher since its viscosity and density are twice as much as hydrogen (Table 2.8). But nevertheless it performs better in H_2O-NH_3 system, literature does not give evidence how a Helium would behave with organic compounds. Therefore, more experiments are needed to establish the influence on the currently used mixture of TEG.DME-R134.

Table 2.8: Thermophysical properties of Helium and Hydrogen [39]

	Mass (g/mol)	Specific Heat ($kJ/kg \cdot K$)	Viscosity ($\mu P_a/s$))	Density (kg/m^3)
Helium	4	5.19	19.850	0.1635
Hydrogen	2	14.312	9.011	0.0823

- **Failure Cause 3: Improper charge**

  Although we can know the system is charged through the glass window of the solution

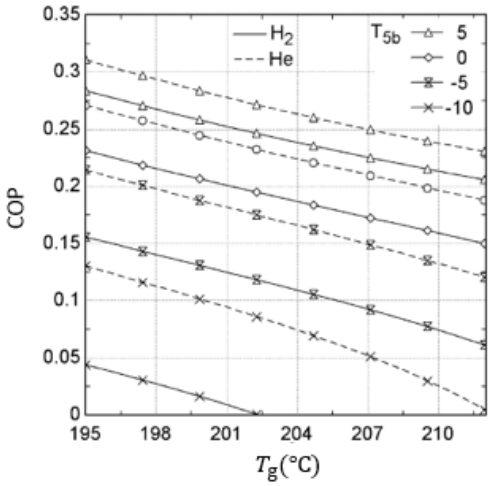

Figure 2.8: A numerical prediction of COP vs. generator temperature and evaporator outlet temperature(T_{5b}) using H_2 and He respectively on an aqua-ammonia DAR system [63].

tank, it should be noted that it is possible to have problems from the improper quantity of charge. A refrigeration machine having an improper charge may exhibit reduced capacity or even not run at all. An undercharged system may tend to lead the generator to operate at an excessively high temperature that can result in failure, and an overcharged machine may cause the solution to boil up over the separator and enter the condenser, on event that would degrade the performance of the system.

Also, the mingled non-condensable gas in the process of charging should be avoided. Internally, the non-condensable cannot only weaken the effect of condensation but can also decrease the refrigerant's partial pressure on the surface of the absorber and decrease the effect of absorption and even stop the absorption further in the absorber.

- **Failure Cause 4: Improper Heat Source**

  Following the prior testing, another consideration was given to the performance of the heating element. This was used to simplify the commissioning, however, the temperature rise from this component is robust and barely controllable, which may be too fast to lead a proper reaction.

  A simple heating experiment to simulate the response in the generator was conducted. The liquid sample (TEG.DME liquid with dissolved R134a) was directly collected from the prototype. Similar to the last testing, the temperature was slightly increased via the variac. Weak bubbles were observed on the surface of the element at temperatures

above 40 °C. When the temperature at the surface of the element was increased to 160 °C, the temperature of the liquid reached only 92°C, followed by weak bubbling and combustion.

This gave information that: there is a significant gap between the temperature of the heat source and the temperature of our working fluid, while the heating process was neither even nor smooth. The heat source from the heating element as a "point heating" was not favourable.

- **Failure Cause 5: Contaminated Working Fluid**

  After all the failure tests performed as described above, chemical decomposition issues were concerned. This can be either contamination of the fluid by external objects, or chemical decomposition.

  It is worthwhile to mention that both the refrigerant and absorbent are soluble in water. TEG.DME may form peroxides during prolonged and careless storage, and should be stored in a tightly closed container and avoid contact with light.

  To gather more information about the sample fluid, a thermogravimetric analysis (TGA) was carried out. Mass loss can be detected during this investigation to verify decomposition, oxidation, or loss of volatiles and it cannot be influenced by pressure. A sample of pure Tetraglyme was analysed. The temperature program was set from 30 °C to 300 °C at 10 °C/minute heating in a Nitrogen atmosphere. As shown in Figure 2.9, the descending TGA thermal curve indicates a weight-loss has occurred. 5 % loss occurs when the temperature reaches 95 °C, and only 1 % of the Tetraglyme is left when the temperature reaches to 178 °C. The diagram of the full results is shown in Appendix A. It was concluded that the liquid used to reach a temperature above 160 °C experienced pyrolysis.

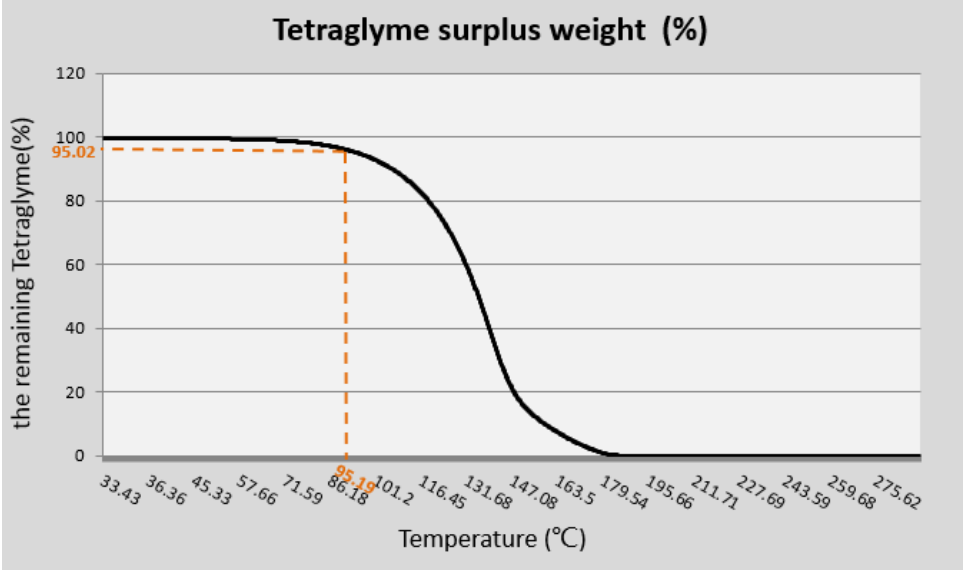

Figure 2.9: Thermogravimetric analysis graph

Chapter 3

Adsorption Cooling Study

3.1 Introduction and aim of the study

Gas-solid interfaced adsorption is most commonly used in cooling aimed adsorption technology. As previously mentioned, compared to the bulk-phenomenon absorption chillers, the surface-based adsorption process, is seen as capable of operating with heat source temperatures as low as 50 °C (the lowest heat source temperature for absorption system being 90 °C [26]), and can use refrigerants having zero ozone depletion potential (ODP) and low global warming potential (GWP) such as methanol and water. Higher efficiency advanced adsorption refrigeration cycles have been developed in the past, namely continuous, heat recovery cycle, mass recovery cycle, and forced convective thermal wave cycle [2]. Due to their solid character, adsorption systems are more viable for vibration applications like vehicles, fishing boats and even space missions.

To provide quasi-continuous commissioning, predecessors of this project, Ana Markovic et al. developed a multi-sorption-bed system, in which half the modules operate a heat recovery process while the others are adsorbing. The study was carried out at Stuttgart University, where the as-built prototype was initially developed for commercial use in an automotive air-conditioning application using methanol and activated carbon. However, the COP of these units is barely satisfactory (Table 1.3).

The key operation in the adsorption systems is the proper analysis and understanding of the heat and mass transfer of the working agents between the components of the unit. The major motivation behind the present work was to investigate the theoretical steady state behaviour

of a basic, intermittent adsorption cycle. The focus was to commission an adsorption unit, working with methanol and activated carbon in order to collect experimental data and create a theoretical model, which would predict its performance. This data was collected at different temperatures in the adsorption process. The Dubinin-Astakhov equation (3.3) was used for fitting the experimental data, from which the adsorption process and the COP can be analysed and calculated. As in all cooling sorption systems, the absorption and adsorption processes are the most crucial processes involving mass and heat transfer. The current investigation is focussed only in the adsorption of methanol vapour into the activated carbon, and not in the desorption process. The theoretical model developed helped the ongoing research of the "Institute of Chemical Process Engineering" in Stuttgart University, on solid adsorption and organic compounds.

3.2 Operating Principle

- **Adsorption mechanism**

  Adsorption is the accumulation of ions, atoms, or molecules from the adsorbate that adhere onto the surface of the solid adsorbent surface. Two types of adsorption processes are considered, which are physisorption and chemisorption. The former reversible physisorption is processed with electrostatic forces, van der Waals forces, and the adsorbate remains chemically stable during the process. In contrast, the latter, chemisorption, is caused by strong interaction between ionic or covalent bonds. The adsorbed molecule is therefore chemically altered in its structure.

- **Working agents**

  Activated carbon (AC) is one of the most exploited and variously applied substances in the current century due to its micro-porosity. Except for its cooling applications, the adsorption of VOCs onto these porous adsorbents has been also widely used for environmental treatment.

  AC is obtained by thermal decomposition (at temperatures lower than 1000 °C) or combustion of carbonaceous source materials, such as charcoal, coconuts, wood, and lignite [7]. In this process, the internal structure of the charcoal particle is eroded, creating an internal network of even smaller pores, which makes the AC two to three times more efficient in its adsorption capability. From these diverse raw materials,

activating agents, and the conditions of the treatment process, a large number of randomly distributed internally connected voids of various shapes and sizes can be formed and used in different fields. Figure 3.1 illustrates a microscopic view of a granular activated carbon sample. Other than the nature of the adsorbate (methanol), and the experimental conditions (temperature and pressure), the adsorption capacity of AC depends heavily on its surface micro-structure. The specific surface area of its micro-pores (radii<2 nm) constitutes about 95 % of the whole surface [7], meso-pores (2 nm<radii<50 nm) and macro-pores (radii>50 nm, frequently in the 500 nm to 2000 nm range), function as transportation routes for adsorbate molecules. In this work, a locally available AC was used, which was manufactured from powdered activated carbon (PAC) extruded with ceramic binder.

	AC sample
Original material	Coconut shell
Shape	Granular
Activated method	Steam
Total porosity (cm^3/g)	0.37
Nominal pore size (nm)	0.73

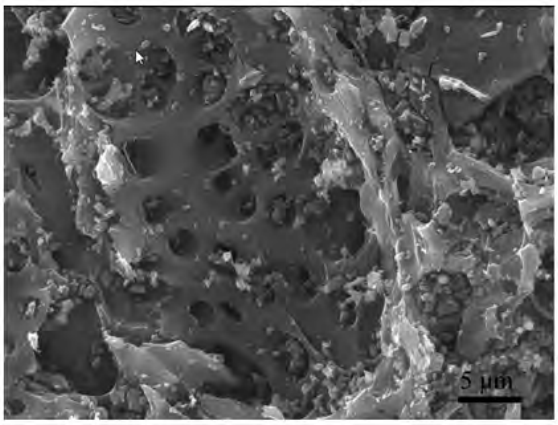

Figure 3.1: Scanning electron microscope (SEM) picture of a sample granular activated carbon from coconut shell [61].

Methanol's small molecular diameter (about 4 $\AA$) allows it be easily adsorbed in micro-pores with a diameter less than 20 $\AA$ [27]. It is adsorbed in to the AC and held by the Van der Waals force. The interaction force is weak and can therefore, be easily reversed by heating or decreasing the pressure. The specific characteristics of the two working pairs are presented in Table 3.1. Since the emphasis of this study is to examine the performance of mass transfer and adsorption behaviour of methanol vapour on monolithic AC. The determination of micro-pore size distribution and material optimisation will not be discussed.

Table 3.1: Adsorption prototype working agents' characteristics [46]

	Methanol
Structural formula	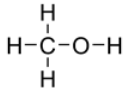
Boiling point (at atm.)	64.7 °C
Critical temperature	239 °C
Density	0.792 g/cm^3
Vapour pressure	13.02 kPa (at 20 °C)
Specific heat capacity (liquid)	2460 J/kg·K (at 20 °C)

	PAC sample
Mass	0.64 g
Thickness	1.15 mm
True density	2.41 g/cm^3 (Hg intrusion)
Total porosity	0.69 (calculated)
Thermal conductivity	0.36 W/m·K (cold/ hot plate)
Specific heat capacity	755 J/kg·K

- **Adsorption cooling cycle**

  The cycle is intermittent and is described best as: a) Desorption-Condensation; b) Evaporation-Adsorption. The cycle illustrated in Figures 3.2a and 3.2b can be described as follows.

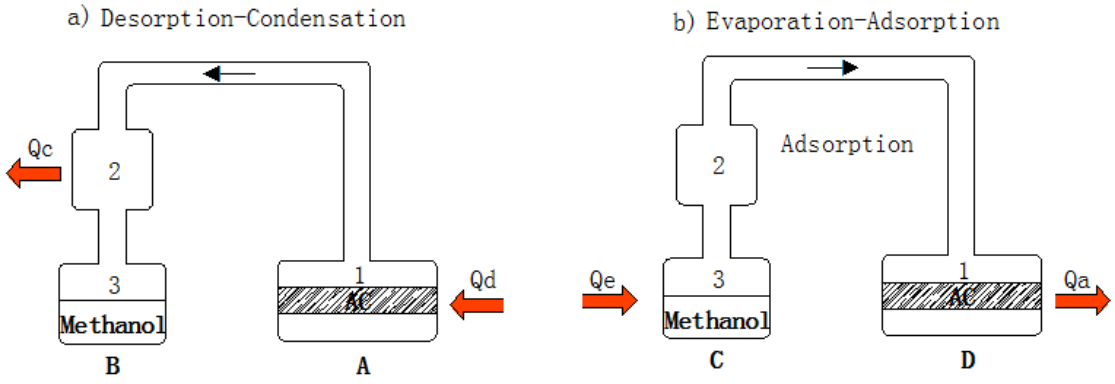

Figure 3.2: Adsorption prototype cooling cycle

Desorption-Condensation

- **State A:**

The activated carbon is saturated with methanol. Heat is received from the external energy (solar-heated water flow is supplied as heat source). The temperature increases and desorption takes place (i.e. vapour methanol leaves the activated carbon).

- **A → B ("compression process"):**
  The pressure increases from evaporating pressure to condensing pressure which is governed by the condenser's lower temperature cooling environment. This step corresponds to the "compression" stage in the vapour-compression cycle.
- **State B:**
  Vapour methanol condenses at the condenser and collected in the liquid receiver.

Evaporation-Adsorption

- **State C:**
  The condenser becomes the evaporator. Heat is received from the surrounding space and the methanol boils and evaporates at the low pressure governed by the adsorber.
- **C → D ("expansion process"):**
  A low pressure environment is created at the adsorption bed, leading to the pressure drop. This is equivalent to the "expansion" step in the vapour-compression cycle. The pressure drop allows the methanol to evaporate at low temperature (saturation temperature) and produce the desired refrigeration effect.
- **State D:**
  Adsorption occurs at the activated carbon bed where the methanol vapours are re-adsorbed in the voids in the carbon. The heat of adsorption generated is extracted to the lower temperature environment.

3.3 Experimental procedure

The as-tested adsorption cooling system is essentially composed of two zones, which are the methanol reservoir-3 (acting as the evaporator/condenser) and the methanol-AC adsorption/desorption bed-1 (acting as the adsorber/desorber) as shown in Figure 3.3. Other components include the vacuum pumps, and several control valves, which are presented in

Figure 3.4.

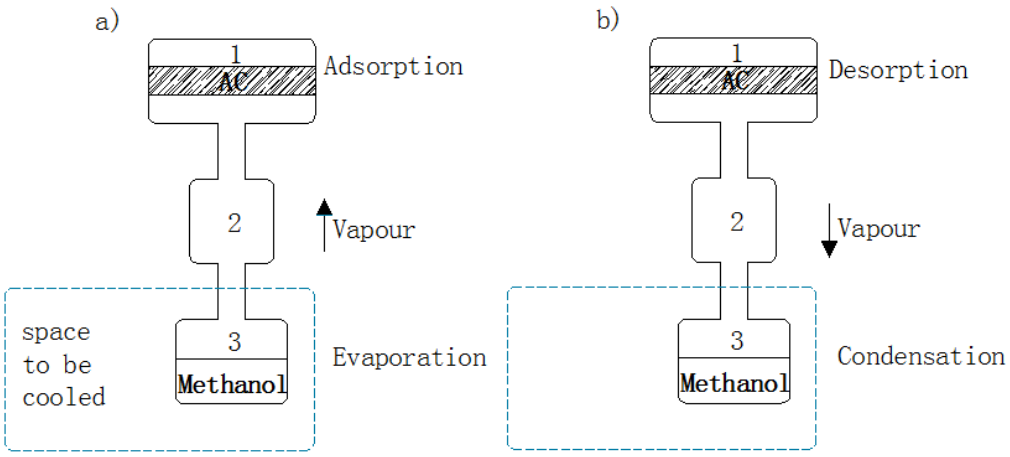

Figure 3.3: Adsorption cooling system. a)-Adsorption process, b)-Desorption process 1: adsorption bed (adsorber/desorber) 2: condenser (only at the desorption process) 3: evaporator

Since pressure in a methanol-AC system is sub-atmospheric, the unit is built with standard high-vacuum parts to ensure that minimum leakage occurs as discussed in Chapter 2.

3.3.1 Charging the unit

Reference is made to the schematic diagram and to the photograph of the unit in Figure 3.4 and Figure 3.5.

For purposes of clarity, chambers V1 and V2 are connected by a valve V-F which remained open during the entire experiment. It was placed in this position for a different reason, which was not part of this study. Henceforth chambers V1 and V2 will be considered as one chamber, named, “dosing chamber”.

A high vacuum was drawn through valve V-A, by the unit’s incorporated membrane vacuum pump, P1, prior to charging with methanol. After the vacuum was drawn, valve V-A was shut.

Liquid methanol is drawn under vacuum into the “degasser” chamber where pure methanol vapour is produced by evaporation. This vapour is introduced into the “dosing chamber”, through the valve V-C, while valve V-E is closed. Fine control of the methanol vapour

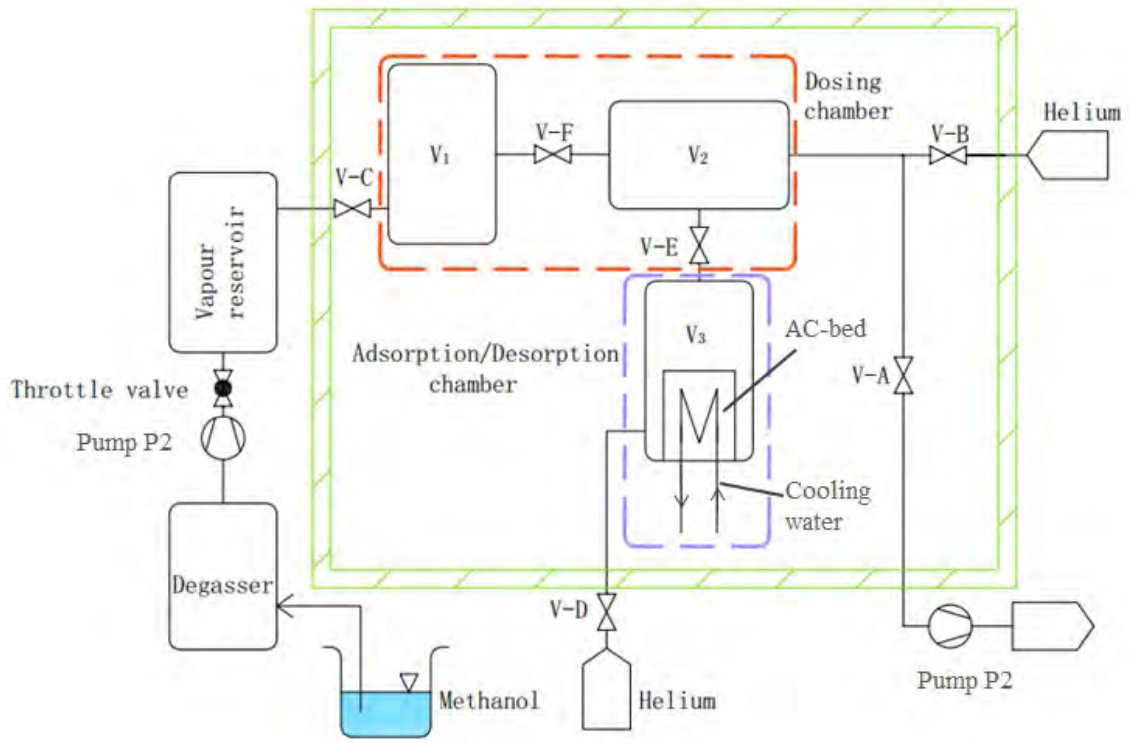

Figure 3.4: Schematic diagram of the experimental set-up

transfer is regulated by the throttle valve, positioned immediately after pump P2. The purpose of the pump P2 is to draw the methanol from the degasser and introduce it into the "vapour reservoir", thus maintaining purity of the vapour.

The dosing chamber, is fitted with a pressure transducer, which indicates when the chamber is filled with the precise mass of methanol.

The adsorption process of the methanol vapour into the "adsorption/desorption chamber" V3 (with built-in activated carbon sample), starts by closing valve V-C and opening valve V-E. The heat generated by the adsorption process is extracted by the cooling water circulating through the adsorption bed (Figure 3.6). Temperature data collected by the thermocouples in the sorption chamber, is plotted, and when the graph shows that equilibrium is reached, the adsorption process of the predetermined methanol vapour has been completed, see Figure 3.7.

The remaining methanol vapour in the dosing chamber is pumped out through valve V-A and the membrane pump P1. To ensure that no methanol vapour is remained in the dosing

chamber, the chamber is purged with helium, which afterwards is also removed through valve V-A and membrane vacuum pump P1.
The helium leftover inside the dosing chamber, after the evacuation process is assumed to be negligible and not influence the adsorption/desorption and evaporation/condensation processes.
Once valves V-B and V-C are closed and valve V-E is opened, the combined dosing chamber V1 and V2 become the condenser or the evaporator chamber, and the chamber V3 becomes the adsorption or the desorption chamber.
To maintain a constant temperature within the reaction environment, the dosing and adsorption/desorption chambers are embedded within a heat-controlled outer shell, and the free space between the various components and the outer shell is filled with aluminium pellets as shown in Figure 3.5. All other parts exterior to the unit were covered with asbestos cloth for insulation purposes.

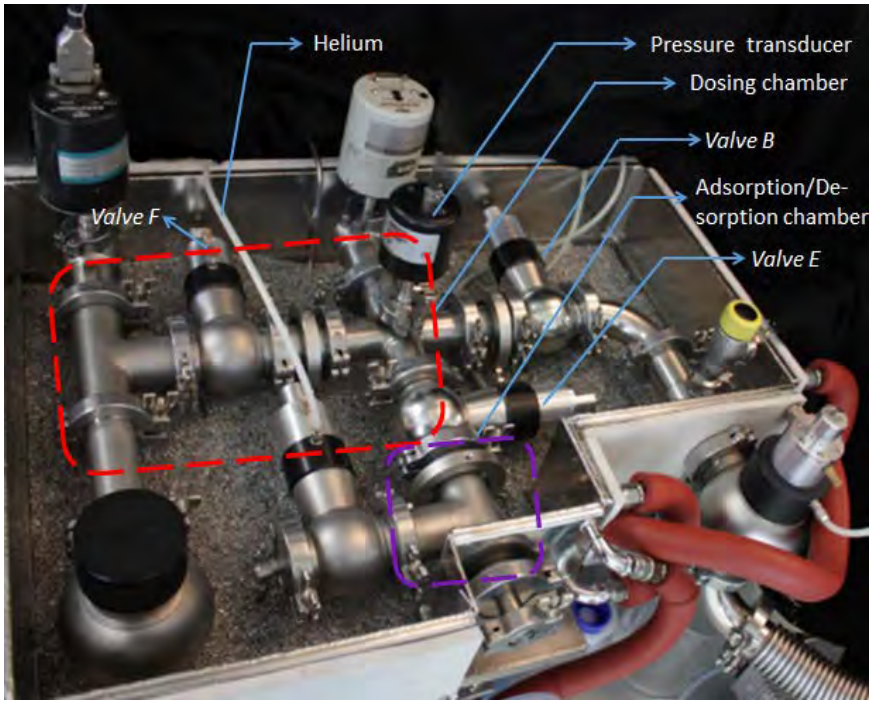

Figure 3.5: Dosing and adsorption/desorption chamber of the adsorption prototype

Figure 3.6 shows the adsorbent/desorbent unit. This unit is embedded into the adsorption/desorption chamber and acts as the testing of the adsorption/desorption processes.

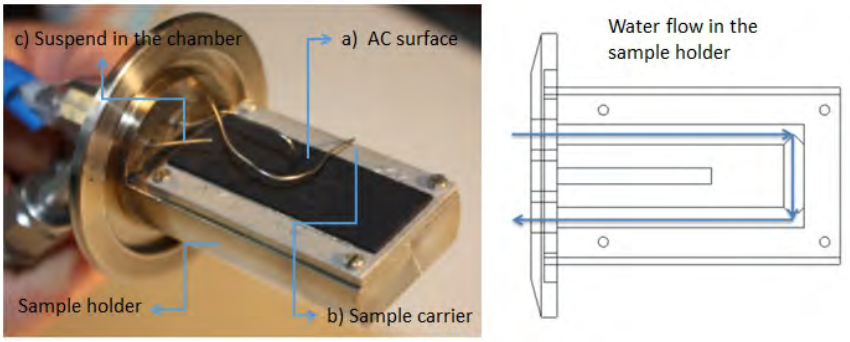

Figure 3.6: Adsorption/desorption chamber, where adsorption/desorption processes occur

Cooling and heating for the adsorption and desorption processes, is provided to this unit by cold and hot water respectively, circulating in the annular space between the carrier of the activated carbon bed and the holding shell. In order to achieve isothermal conditions inside the activated carbon bed throughout the adsorption and desorption processes, this unit was designed to be of small size; consequently all the other components of the system were sized accordingly.

Figure 3.6 also shows the position of the three thermocouples monitoring the temperature during the process at: a) the surface of the AC, b) the casing of the AC-sample carrier, and c) the vapour space above the AC. Figure 3.7 shows the temperature response of the chamber, initially at a temperature of 30 °C.

3.4 Mass And Heat Transfer Performance

In this section, the mass transfer of the methanol to the activated carbon (AC) sample is presented, with aim of showing data, which would assist in generating an accurate theoretical model of the adsorption/desorption processes and thereby predict its performance as aforementioned. The schematic diagram of the experimental set-up is shown in Figure 3.4. The adsorption-desorption process and the operation procedures are intermittent. To obtain the experimental data efficiently, an open-close mechanism for the valves and a data capturing approach were graphically programmed and computer-controlled by the software “Test.con” (Gantner Instruments).

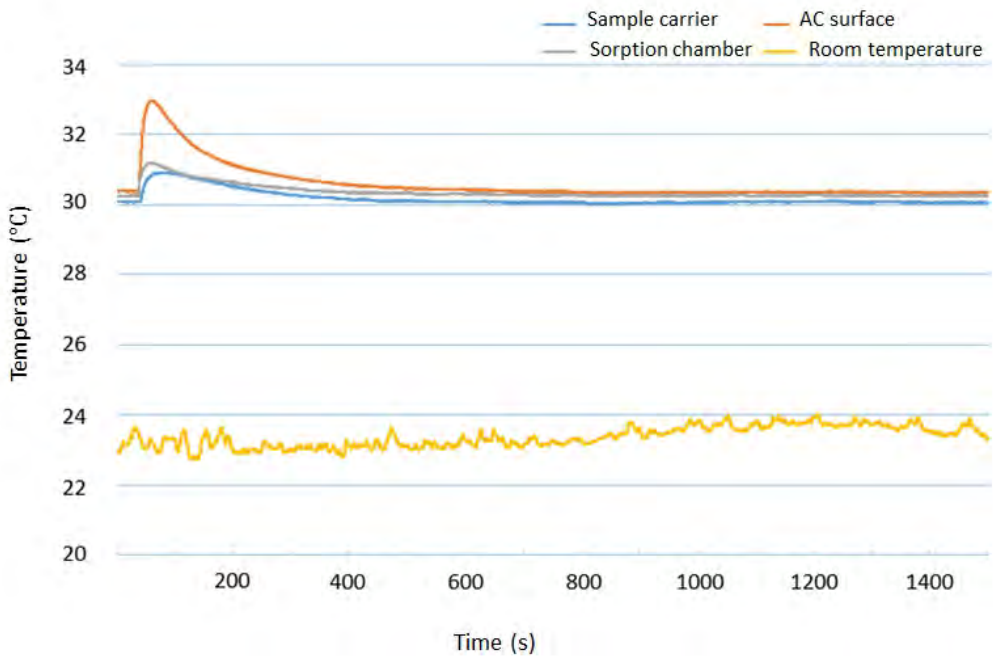

Figure 3.7: Adsorption temperature responses at the AC measurement chamber

3.4.1 Data acquisition procedure

Figure 3.8 demonstrates the computer-control flow of the apparatus (valves alphabet reference to Figure 3.4). Temperature and pressure data were captured automatically every 0.1 second.

- **Preparation**

  The preparation procedure is explained in section 3.3.2

- **Dosing**

  Valve C is set between the vapour reservoir and the dosing chamber. Vapour methanol is released into the dosing chamber by opening valve C till the dosing chamber is filled (valve F is always open, which means V1 + V2 is the dosing chamber as a whole). The dosing process is completed when the pressure inside the dosing chamber has reached the pressure value set by the control program. This set pressure is the saturation pressure of methanol at conditions prevailing in the dosing chamber when it becomes the condenser during operation process, (refer to Figure 3.2a). When this pressure has been reached and recorded, valve V-C is closed and, the status data is saved.

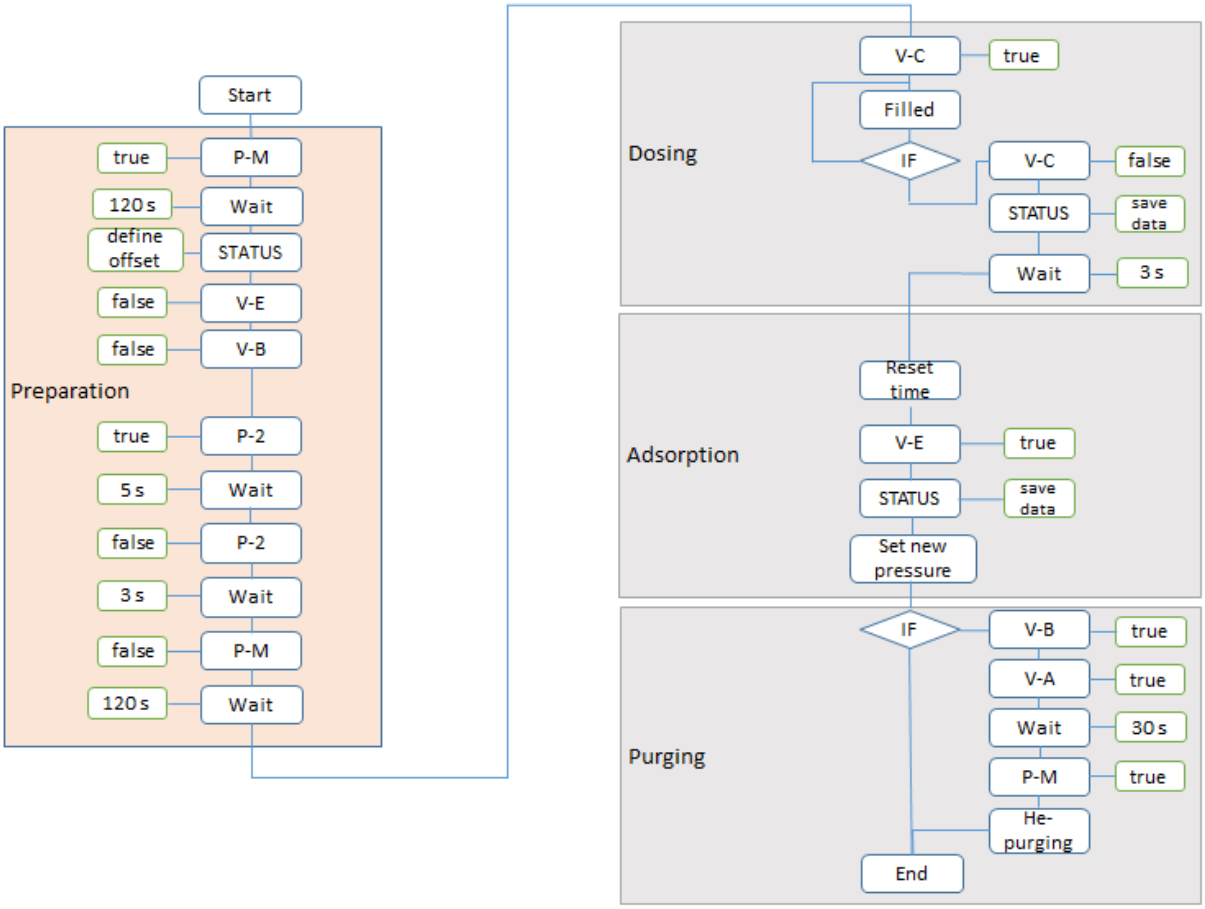

Figure 3.8: Flow chart of the valves and pumps control in the adsorption prototype during the charging up (preparation) and test operation procedures.

- **Adsorption**

  Adsorption starts when the valve E is opened (V-E true), and the vapour methanol starts gaining access to the activated carbon sample (measurement chamber, Figure 3.4). The temperature response curves are tracked till the equilibrium is reached.

- **Purging**

  After each experiment, the adsorbed vapour in chamber V3 is evacuated, by using the membrane pump P1, for 24 hours until the pressure is stable. Then helium is used to purge the dosing and V3 chambers through valves V-B and V-E and facilitating dispersion due to its chemically inert nature . The last step is to open the valves V-A and V-B (V-A and V-B true) and to operate the membrane pump P1 to draw vacuum of the measurement chamber V3, in preparation for the next testing run.

3.4.2 Mass And Heat Transfer Analysis

Adsorption isotherms

With the adsorption process, an equilibrium is reached when the rate of adsorption and the rate of desorption are balanced (Figure 3.9). At this point, the gas-solid system is seen to be in adsorption equilibrium because the number of molecules adhering to the adsorbent surface is equal to the number of molecules escaping from the surface [7].

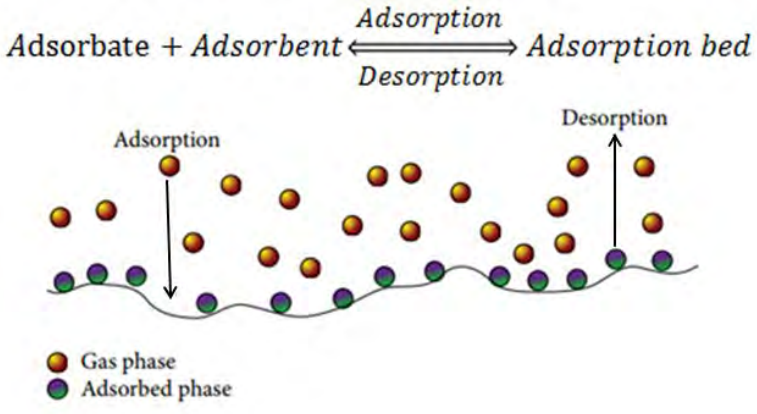

Figure 3.9: Adsorption equilibrium dynamics [19]

The adsorption process or the equilibrium relationship is usually described using isotherm

graphs, which are also utilised as empirical models for fitting the isotherms that are found in the lab tests. The isotherm depicts the amount of the adsorbate adsorbed on the surface of adsorbent as a function of the pressure at a constant temperature. Several models describing the process are most commonly observed, namely: Freundlich isotherm, Langmuir isotherm, and BET (Brunauer-Emmett-Teller) isotherm [16].

In particular, Langmuir isotherms are used to accurately describe the gas-solid-phase adsorption onto activated carbon as in Figure 3.10, which shows an adsorption isotherm plot of Nitrogen on AC at 77 K [35]. It demonstrates that the surface coverage increases with the partial pressure of the adsorbents. The isotherm was published in 1916 [21], depicting a mono-layer adsorption by assuming that the adsorbate behaves as ideal gas.

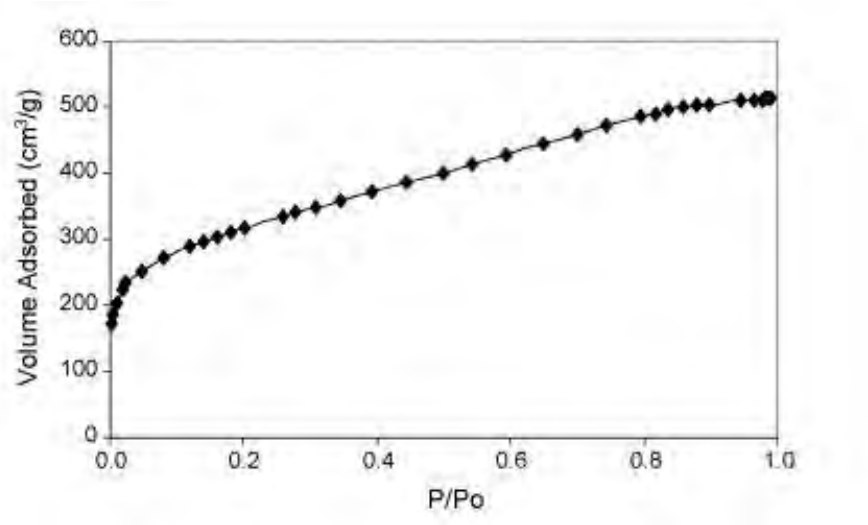

Figure 3.10: Langmuir adsorption isotherm of Nitrogen on AC at 77 K [35]

This happens when a constancy of pressure or temperature inside the adsorption chamber is observed. Adsorption equilibrium was then measured using the volumetric method, (manometry). Adsorbed loading is of equivalence as a pressure difference between the initial and final equilibrium pressure, described by the equation below.

$$m = (P_0 V_0 - P_{eq} V_{eq})/RTM \tag{3.1}$$

In the set-up under investigation, the initial pressure of the dosing chamber is known. This pressure is assumed to be the saturation pressure of methanol at the dosing chamber when it is acting as a condenser during the desorption phase of the system. With reference to

Figure 3.4, the adsorbed amount can be computed by:

$$m = (P_0(V_1 + V_2) - P_{eq}(V_1 + V_2 + V_3 - V_{ac}))/RTM \tag{3.2}$$

Where

m is the weight of the AC sample,

P_0 is the initial pressure in the methanol vapour reservoir in $V_1 + V_2$ (before opening valve V-E),

V_3 is the volume of the recipient reservoir (measurement chamber),

V_{ac} is the volume of AC sample,

P_{eq} is the equilibrium pressure in $V_1 + V_2 + V_3$.

Equation 3.2, together with the data collected from the dosing and adsorption/desorption chamber V_3 were fed into MATLAB, and the isotherms derived in temperatures of 30 °C and 60 °C are shown in Figure 3.11. The measured pressure data represents the adsorption

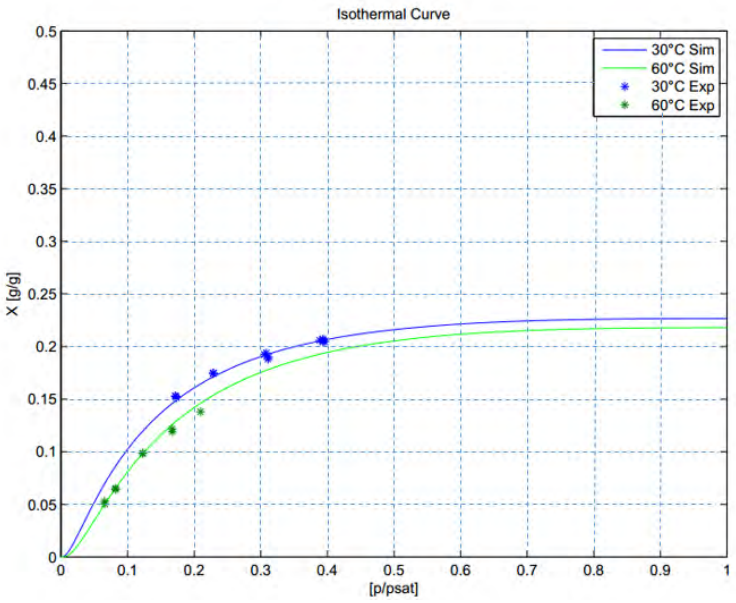

Figure 3.11: Adsorption isotherms of methanol-AC

behaviour at the particle level in the adsorption chamber. The adsorption rate continues to decrease with the increasing coverage of the AC surface by the methanol molecules. The predicted pressure-concentration behaviour and the measured pressure data have good

correlation. From Figure 3.11, it can also be seen that at the initial adsorption process, the isotherm for 30 °C has a steeper slope than the 60 °C isotherm curve. This indicates that the adsorption rate decreases with the increase of temperature.

Dubinin-Astakhov-Theory

The Dubinin-Astakhov (DA) theory has wide application for the methanol-AC system to evaluate adsorption equilibrium in microporous material like AC [25]. As for physical adsorption of gasses on micro-porous solids, it permits the calculation of the surface area and the pore volume distribution, if:

1. The area of AC occupied by a single adsorbed molecule is known;
2. The number of adsorbed molecules of a fluid that covers the adsorbent with a monomolecular layer could be determined;
3. Surface area available to the adsorbate molecules could be calculated.

Its equation is one of the most popular isotherm equations in adsorption theory. It is about the volume filling of micro-pores, the analysis of the capillary structure, and was found to be the most ideal isotherm to simulate experimental data. The experimental data was used to evaluate the isotherms by using the DA theory to characterise the strength of the adsorbent-adsorbate affinity. The equation is expressed as:

$$W = W_0 exp[-[bRTln(P_s/P_{eq})]^n] \tag{3.3}$$

Where the meanings of the variables are:
$W(cm^3/g)$ = the volume of the micro-pores filled with the adsorbate;
$W_0(cm^3/g)$ = the maximum volume of the adsorbent micro-pores (maximum loading);
P_{eq} = the equilibrium pressure;
P_s = saturated pressure corresponding to the adsorbent temperature T;
Parameters b and n depend on the chosen adsorbent/adsorbate pair.
Equation 3.3 can be re-written as :

$$W = W_0 exp(-(A(E_a))^n) \tag{3.4}$$

Where $A = RTln(P_0/P)$ is the adsorption potential energy (J/g) on the adsorbent surface pores;

n and E depend on the different adsorbate-adsorbent pair and are temperature-based parameters. It was mentioned by Stoeckli [44] that the exponent value n=2∼3 for homogeneous carbons, n<2 for heterogeneous active carbons and n>4 for zeolites.

The potential energy is a function of the position in the pore. This enables the characteristic curves (plots of W/W_0 versus A) of different adsorptives on the same solid to be superimposed.

The aim of this work was to establish the values of n, where a satisfactory agreement could be obtained between experimental adsorption data and the DA equation 3.4, thereby trying to verify the obtained DA parameters referring to related results calculated.

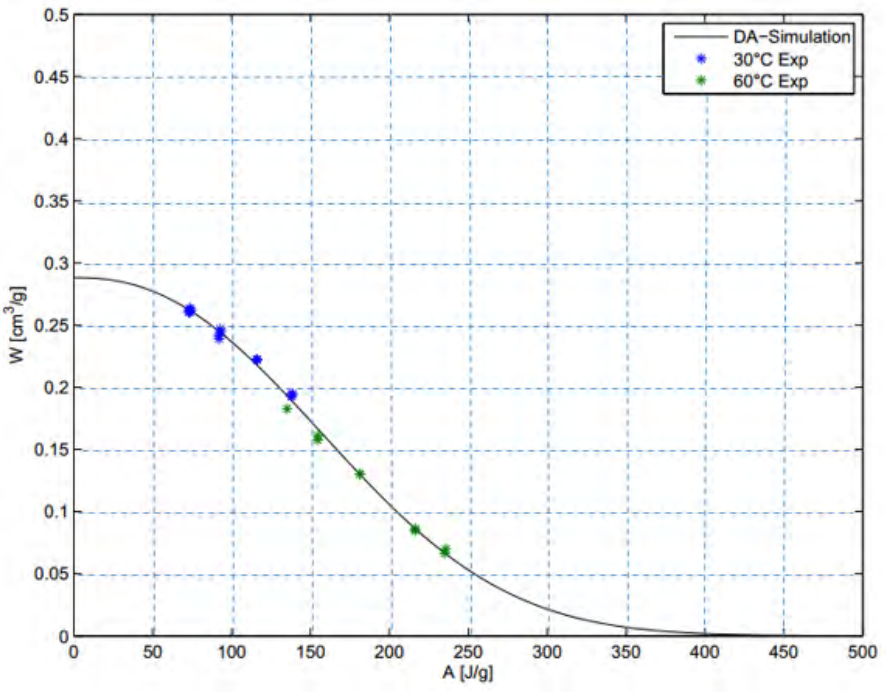

Figure 3.12: Adsorbed micro-pore volume as a function of adsorption potential for the tested sample

A MATLAB program was developed based on equation 3.2 and 3.4 to use captured experimental pressure data and predict the performance by:

1. Converting experimental data from data-type(.txt) to Matlab data-type(.dat).
2. Generating prediction with the pressure data for graphic presentation.

The detailed code can be found in Appendix F.

From the result in Figure 3.12, a satisfactory agreement is seen between the experimental adsorption data and the DA simulation. This programme can be used to predict and linearise methanol-AC adsorption data over different ranges of relative pressure on an adsorption isotherm.

The validation of the experimental data against the standard adsorption isotherms are hereby completed. As a regression approximation, this is of long-standing importance for an accurate data correlation, as well as a true reflection of the activated carbon adsorption capability.

Chapter 4

Conclusions and Future Work

Both absorption and adsorption cooling methods were investigated. A further understanding of the sorption processes from the macroscopic to the microscopic scales was achieved.
Some problems arose when running the absorption prototype, causing break-down of the experimental procedures. These were discussed in the text, from which, the following conclusions are drawn.
It is of importance that heat is supplied evenly over the surface of the heating element. A heating element may have surface "hot-spots", which could denature the absorbent and render it unable to absorb the refrigerant. The pyrolysis temperature for Tetraglyme was verified to be 95 °C, hence the operation of any absorption system with TEG.DME should not be higher than this value.
In spite of the absorption hardware difficulties encountered during construction and further during its testing, thermodynamic and equilibrium properties show that such a system is of potential use at low generator temperatures.
With respect to the adsorption section, temperature dependent experiments of methanol adsorption on monolithic activated carbon were carried out and pressures were recorded, which gave rise to estimation of the methanol concentration in the activated carbon. It was concluded that faster adsorption equilibrium was observed at a lower temperature for the same concentration. Mass transfer and adsorption kinetics parameters were fitted to the pressure-temperature experimental data, which verified Dubinin-Astakhov equation's applicability to characterise methanol-AC adsorption equilibrium.
The study focussed mainly on prototype testing, and the design of these units was based

on their thermodynamic parameters and experimental data. The data and the theoretical model developed are in agreement, allowing precise prediction of methanol-AC adsorption process.

Bibliography

[1] Albert, E. and Leo, S. *Refrigeration*. US Patent 1,781,541. 1930.

[2] Alghoul, M., Sulaiman, M., Azmi, B., and Wahab, M. A. "Advances on multipurpose solar adsorption systems for domestic refrigeration and water heating". *Applied thermal engineering* 27.5 (2007), pp. 813–822.

[3] Allouhi, A, Kousksou, T, Jamil, A, El Rhafiki, T, Mourad, Y, and Zeraouli, Y. "Optimal working pairs for solar adsorption cooling applications". *Energy* 79 (2015), pp. 235–247.

[4] Anyanwu, E. "Review of solid adsorption solar refrigeration II: An overview of the principles and theory". *Energy Conversion and Management* 45.7 (2004), pp. 1279–1295.

[5] Arivazhagan, S, Murugesan, S., Saravanan, R, and Renganarayanan, S. "Simulation studies on R134a-DMAC based half effect absorption cold storage systems". *Energy Conversion and anagement* 46.11 (2005), pp. 1703–1713.

[6] Balaras, C. A., Grossman, G., Henning, H.-M., Ferreira, C. A. I., Podesser, E.,Wang, L., and Wiemken, E. "Solar air conditioning in Europe–an overview". *Renewable and sustainable energy reviews* 11.2 (2007), pp. 299–314.

[7] Bansal, R. and Goyal, M. *Activated Carbon Adsorption*. CRC Press, 2005.

[8] Benhmidene, A., Chaouachi, B., and Gabsi, S. "Effect of operating conditions on the performance of the bubble pump of absorption-diffusion refrigeration cycles". *Thermal Science* 15.3 (2011), pp. 793–806.51

[9] Borde, I, Jelinek, M, and Daltrophe, N. "Absorption system based on the refrigerant R134a". *International Journal of Refrigeration* 18.6 (1995), pp. 387–394.

[10] Castillo, J. M., Silvestre-Albero, J., Rodriguez-Reinoso, F., Vlugt, T. J., and Calero, S. "Water adsorption in hydrophilic zeolites: experiment and simulation". *Physical Chemistry Chemical Physics* 15.40 (2013), pp. 17374–17382.

[11] Cengel, Y. and Boles, M. *Property Tables Booklet for Use with Thermodynamics: An Engineering Approach*. McGraw-Hill series in mechanical engineering. McGraw-Hill, 2001.

[12] Dannen, G. "The Einstein-Szilárd refrigerators". *Scientific American* 276.1 (1997), pp. 90–95.

[13] Dieng, A. and Wang, R. "Literature review on solar adsorption technologies for ice-making and air-conditioning purposes and recent developments in solar technology". *Renewable and Sustainable Energy Reviews* 5.4 (2001), pp. 313–342.

[14] Ehrismann, B. *Collated and updated list of solar cooling installations in participating countries*.

[15] El-Sharkawy, I. I., AbdelMeguid, H., and Saha, B. B. "Potential application of solar powered adsorption cooling systems in the Middle East". *Applied Energy* 126 (2014), pp. 235–245.

[16] Faeth, P. "Adsorption and vacuum technique" (1962).

[17] Fernandes, M., Brites, G., Costa, J., Gaspar, A., and Costa, V. "Review and future trends of solar adsorption refrigeration systems". *Renewable and Sustainable Energy Reviews* 39 (2014), pp. 102–123.

[18] Georg, M. C. and Von, P. B. C. *Refrigerator*. US Patent 1,685,764. 1928.

[19] Hassan, H. "Energy analysis and performance evaluation of the adsorption refrigeration system". *ISRN Mechanical Engineering* 2013 (2013).

[20] Kai Wang Edward A. Vineyard, P. "Adsorption refrigeration". *ASHRAE Journal* (2011).

[21] Keller, J. and Staudt, R. *Gas Adsorption Equilibria: Experimental Methods and Adsorptive sotherms*. Springer ebook collection / Chemistry and Materials Science 2005-2008. Springer US, 2006.

[22] Kim, D. and Ferreira, C. I. "Solar refrigeration options–a state-of-the-art review". *International Journal of refrigeration* 31.1 (2008), pp. 3–15.

[23] Kouremenos, D. and Stegou-Sagia, A. "Use of helium instead of hydrogen in inert gas absorption refrigeration". *International journal of refrigeration* 11.5 (1988), pp. 336–341.

[24] Kouremenos, D., Stegou-Sagia, A, and Antonopoulos, K. "Three-dimensional evaporation process in aqua-ammonia absorption refrigerators using helium as inert gas". *International journal of refrigeration* 17.1 (1994), pp. 58–67.

[25] Leite, A. P. F., Belo, F. A., Martins, M. M., and Riffel, D. B. "Central air conditioning based on adsorption and solar energy". *Applied Thermal Engineering* 31.1 (2011), pp. 50–58.

[26] Li, T., Wang, R., and Li, H. "Progress in the development of solid–gas sorption refrigeration thermodynamic cycle driven by low-grade thermal energy". *Progress in Energy and Combustion Science* 40 (2014), pp. 1–58.

[27] Li, Z. and Sumathy, K. "A solar-powered ice-maker with the solid adsorption pair of activated carbon and methanol". *International Journal of Energy Research* 23.6 (1999), pp. 517–527.

[28] LindeAG. *Managing refrigerants the responsible way*. Tech. rep.

[29] Louajari, M., Mimet, A., and Ouammi, A. "Study of the effect of finned tube adsorber on the performance of solar driven adsorption cooling machine using activated carbon–ammonia pair". *Applied energy* 88.3 (2011), pp. 690–698.

[30] Ltd, S. S. *Refrigeration Technology*. url: https://www.downloads.siemens.com / download - center / Download . aspx ? pos = download \ &fct = getasset \&id1=8359.

[31] Marcriss, R., Gutraj, J., and Zawacki, T. “Absorption fluid data survey: final report on worldwide data, ORLN/sub/8447989/3, Inst”. *Gas Tech* (1988).

[32] Mendes, L. and Collares-Pereira, M. “A solar assisted and air cooled absorption machine to provide small power heating and cooling”. *International Sorption Heat Pump Conference, Munich, Germany*. 1999, pp. 129–136.

[33] Miles, D. J., Sanborn, D. M., Nowakowski, G. A., and Shelton, S. V. “Gas fired sorption heat pump development”. *Heat Recovery Systems and CHP* 13.4 (1993), pp. 347–351.

[34] Narayankhedkar, K. and Maiya, M. P. “Investigations on triple fluid vapour absorption refrigerator”. *International journal of refrigeration* 8.6 (1985), pp. 335–342.

[35] Önal, Y. “Kinetics of adsorption of dyes from aqueous solution using activated carbon prepared from waste apricot”. *Journal of hazardous materials* 137.3 (2006), pp. 1719–1728.

[36] Paurine, A, Maidment, G., Eames, I., Missenden, J, and Day, A. “A REVIEW OF "PUMPLESS" ABSORPTION REFRIGERATION CYCLES”.

[37] Rathore, M. and Kapuno, R. *Engineering Heat Transfer*. Jones & Bartlett Learning, 2011.

[38] Rezk, A. R. and Al-Dadah, R. K. “Physical and operating conditions effects on silica gel/water adsorption chiller performance”. *Applied Energy* 89.1 (2012), pp. 142–149.

[39] Rodríguez-Muñoz, J. and Belman-Flores, J. “Review of diffusion–absorption refrigeration technologies”. *Renewable and Sustainable Energy Reviews* 30 (2014), pp. 145–153.

[40] Santori, G., Santamaria, S., Sapienza, A., Brandani, S., and Freni, A. “A standalone solar adsorption refrigerator for humanitarian aid”. *Solar energy* 100 (2014), pp. 172–178.

[41] Shelton, S. V., Stewart, S. W., Erickson, D., et al. “Bubble pump design for single pressure absorption refrigeration cycles”. *ASHRAE Transactions* 108.1 (2002), pp. 867–876.

[42] Solmuş, İ., Yamalı, C., Kaftanoğlu, B., Baker, D., and Çağlar, A. "Adsorption properties of a natural zeolite–water pair for use in adsorption cooling cycles". *Applied energy* 87.6 (2010), pp. 2062–2067.

[43] Srikhirin, P., Aphornratana, S., and Chungpaibulpatana, S. "A review of absorption refrigeration technologies". *Renewable and sustainable energy reviews* 5.4 (2001), pp. 343–372.

[44] Stoeckli, H. and Kraehenbuehl, F. "The enthalpies of immersion of active carbons in relation to the Dubinin theory for the volume filling of micropores". *Carbon* 19.5 (1981) pp. 353–356

[45] Tamainot-Telto, Z and Critoph, R. "Adsorption refrigerator using monolithic carbon-ammonia pair". *International Journal of Refrigeration* 20.2 (1997). pp. 146–155.

[46] Touloukian, Y. and Vargaftik, N. *Handbook of Physical Properties of Liquids and Gases: Pure Substances and Mixtures*. Springer Berlin Heidelberg, 2014.

[47] Tozer, R. M. and James, R. W. "Fundamental thermodynamics of ideal absorption cycles". *International journal of refrigeration* 20.2 (1997), pp. 120–135.

[48] Ullah, K., Saidur, R, Ping, H., Akikur, R., and Shuvo, N. "A review of solar thermal refrigeration and cooling methods". *Renewable and Sustainable Energy Reviews* 24 (2013), pp. 499–513.

[49] Vasiliev, L., Mishkinis, D., Antukh, A., and Vasiliev Jr, L. "Solar-gas solid sorption refrigerator". *Adsorption* 7.2 (2001), pp. 149–161.

[50] Vicatos, G and Bennett, A. "Multiple lift tube pumps boost refrigeration capacity in absorption plants". *Journal of Energy in Southern Africa* 18.3 (2007), pp. 49–57.

[51] Vicatos, G. *Heat and mass transfer characteristics: Design and optimisation of absorption refrigeration machines*. PhD Thesis, UCT, 1995.

[52] Wang, D., Li, Y., Li, D, Xia, Y., and Zhang, J. "A review on adsorption refrigeration technology and adsorption deterioration in physical adsorption systems". *Renewable and Sustainable Energy Reviews* 14.1 (2010), pp. 344–353.

[53] Wang, D., Zhang, J., Tian, X., Liu, D., and Sumathy, K. "Progress in silica gel–water adsorption refrigeration technology". *Renewable and Sustainable Energy Reviews* 30 (2014), pp. 85–104.

[54] Wang, L., Wang, R., Lu, Z., Chen, C., Wang, K, and Wu, J. "The performance of two adsorption ice making test units using activated carbon and a carbon composite as adsorbents". *Carbon* 44.13 (2006), pp. 2671–2680.

[55] Wang, R., Wang, L., and Wu, J. *Adsorption Refrigeration Technology: Theory and Application*. Wiley, 2014.

[56] Wang, R. and Oliveira, R. "Adsorption refrigeration-an efficient way to make good use of waste heat and solar energy". *Progress in Energy and Combustion Science* 32.4 (2006), pp. 424–458.

[57] Wang, R., Wu, J., Xu, Y., Teng, Y, and Shi, W. "Experiment on a continuous heat regenerative adsorption refrigerator using spiral plate heat exchanger as adsorbers". *Applied thermal engineering* 18.1 (1998), pp. 13–23.

[58] Wang, R., Wu, J., Xu, Y., and Wang, W. "Performance researches and improvements on heat regenerative adsorption refrigerator and heat pump". *Energy conversion and management* 42.2 (2001), pp. 233–249.

[59] Wu, J., Wang, R., and Xu, Y. "Dynamic simulation and experiments of a heat regenerative adsorption heat pump". *Energy conversion and management* 41.10 (2000), pp. 1007–1018.

[60] Xi, H., Luo, L., and Fraisse, G. "Development and applications of solar-based thermoelectric technologies". *Renewable and Sustainable Energy Reviews* 11.5 (2007), pp. 923–936.

[61] Xu, D., Zhang, J., Li, G., Xiao, P., Webley, P., and Zhai, Y.-C. "Adsorption equilibrium and kinetics of CO (2) and H (2) O on activated carbon". *Wuji Cailiao Xuebao(Journal of Inorganic materials)* 27.2 (2012), pp. 139–145.

[62] Yokozeki, A. "Theoretical performances of various refrigerant–absorbent pairs in a vapour-absorption refrigeration cycle by the use of equations of state". *Applied Energy* 80.4 (2005), pp. 383– 399.

[63] Zohar, A, Jelinek, M, Levy, A, and Borde, I. "Numerical investigation of a diffusion absorption refrigeration cycle". *International Journal of Refrigeration* 28.4 (2005), pp. 515–525.

Appendices

Appendix A: TEG.DME thermogravimetric analysis result

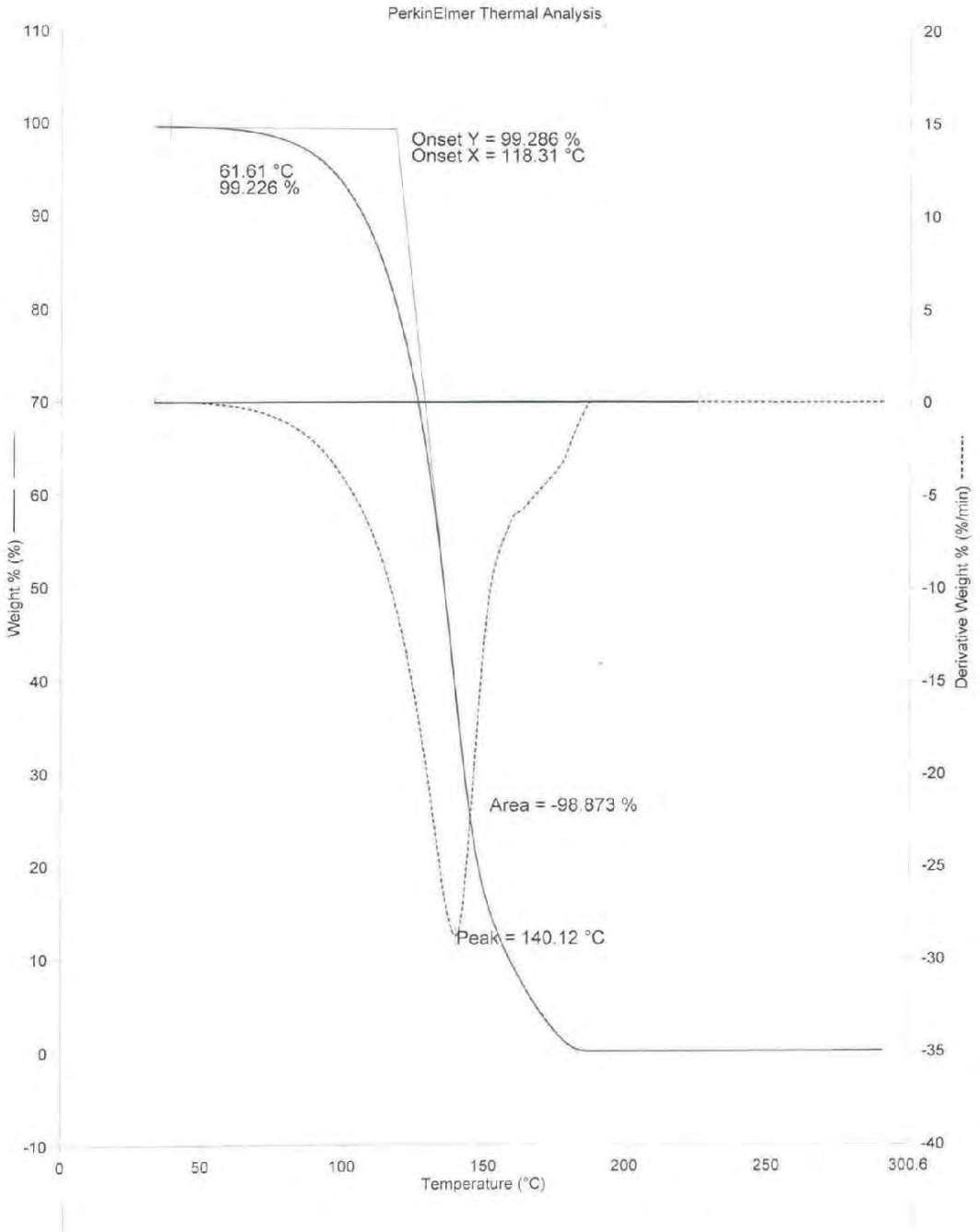

Appendix B: Certificate of prototype pressure testing

Marine & Industrial
Allweld

2 Diesel Road, Ndabeni • PO Box 145, Howard Place, 7450, Cape Town, South Africa
Tel: +27 (0)21 511 7473 • Fax: +27 (0)21 511 9409 • Website: www.allweld.co.za • Email: info@allweld.co.za
Vat No: 4800172290 • CK No: 2008/005168/07

Pressure Test Certificate

Client	: University of Cape Town
Client Order No.	: Meihua Jin
Job No.	: JN 1002251
Description	: Absorption refrigeration unit
Date	: 11 March 2014
Gauge No.	: AV05
Medium	: Nitrogen
Duration	: 20 Mins
Remarks	: Unit passed at 20 Bar pressure for 20minutes

ALLWELD
Name : W.J. Rock ALLWELD QC 1
Signature : Signed

Witness
Name : Meihua Jin

Signature : Signed

FQ015 30/03/2011 Rev:1

Appendix C: Design calculations

Subscripts:

c: condenser;
cr: refrigerant states at the condenser;
cw: cooling water states at the condenser;

pc: pre-cooler;
pcr: refrigerant states at the pre-cooler;
pcw: cooling water states at the pre-cooler;

e: evaporator;
er: refrigerant states at the evaporator;
ew: cooling water states at the evaporator;

a: absorber;
ar: refrigerant states at the absorber;
aw: cooling water states at the absorber;

Given:

Table C-1: Prototype basic design parameters

Parameters	Assumed values
Refrigeration capacity	100 W
Condenser temperature	40 ℃
Pre-cooler temperature	15 ℃
Evaporator temperature	-5 ℃

Table C-2: Selected pipe sizes

Parameters	Pipe sizes
Condenser	$D_o = 5/8''$ (15.88 mm), 0.71mm thickness $D_i = 3/8''$ (9.53 mm), 0.57 mm thickness
Pre-cooler	
Evaporator	
Absorber	$D_{ao} = 7/8''$ (22.23 mm), 0.81mm thickness $D_{ai} = 5/8''$ (15.88 mm), 0.71mm thickness
Solution heat exchanger	$D_{exo} = 3/4''$ (19.5 mm), 0.71mm thickness $D_{exi} = 1/2''$ (12.7 mm), 0.61mm thickness
Generator	$D_{go} = 7/8''$ (22.23 mm), 0.81mm thickness

Appendix C: Design calculations

Enthalpy values can be discerned directly from the R134a P-h diagram from Appendix E.

Table C-3: Refrigerant enthalpy values at main points

state point enthalpy	refrigerant conditions	temperature (℃)	enthalpy value (kJ/kg)
h_2	superheat vapour at the inlet of the condenser	90	375
h_{st}	saturated vapour at the condenser	40	322
h_3	de-superheated vapour at the outlet of the condenser	40	158
$h_4 = h_5$	saturated liquid at the outlet of the pre-cooler and the inlet of the evaporator	15	123
h_6	saturated vapour at the outlet of the evaporator	-5	298

From the values above and the Figure 2.6, it can be known that:

$\Delta h_e = h_6 - h_5 = 298 - 123 = 175$ kJ/kg,
$\Delta h_c = h_3 - h_2 = 158 - 375 = -217$ kJ/kg,
$\Delta h_{pc} = h_4 - h_3 = -35$ kJ/kg,
$h_7 = h_6 - \Delta h_{pc} = 333$ kJ/kg.

1. EVAPORATOR:

1.1 Select pipes:

Since a laminar flow regime is expected due to low mass flow rate. A plot of Reynolds number at different diameters was used and showed that tubes with diameters that bigger than 2 mm is suitable.

According to the available industrial-standard copper pipe sizes and related strength analysis, inner pipes with a diameter of $3/8''(9.53\,\text{mm})$ and outer pipes with a diameter of $5/8''(15.88\,\text{mm})$ were selected for the evaporator and the condenser, both of which are outer diameters with thickness of 0.57 mm and 0.71 mm respectively. Other dimension can be found in Table C-2.

1.2 Estimate the pipe length:

The first law is applied for open systems, assuming steady flow and negligible changes in kinetic and potential energies; each component has one inlet and one outlet. Thus our first law for each device is:

$$\dot{Q} = \dot{W} + \dot{m}(h_{out} - h_i) \quad (1)$$

Since there is no work in the evaporator, we can find the heat removed from the refrigerated space (the evaporator) as follows.

$$\dot{Q} = \dot{m}(h_{out} - h_i) \quad (2)$$

Appendix C: Design calculations

1.2.1 Confirm the mass flow rates at the state of the evaporator:

$$\dot{m}_{er} = \frac{\dot{Q}}{\Delta h_e} \tag{3}$$

$$\dot{m}_{er} = \frac{100\ W}{17500\ J/kg} = 0.00057\ kg/s$$

Since the amount of heat lost by the refrigerant equals to the amount of heat gained by the water, we can get $\dot{m}_{ew}$ from the heat transfer formula below:

$$\dot{Q} = \dot{m} C \Delta T \tag{4}$$

Where
C = the specific heat, which for water is 4.189 kJ/kg · K,
ΔT = the changed temperature.
As mentioned in the previous chapters, the inlet water temperature is estimated as residential water temperature of 18 ℃ and ΔT_{ew} is 10 ℃. At the average of 13 ℃, it can be found that C_{ew} = 4.189 kJ/kg · K from Appendix D.

$$\therefore \dot{m}_{ew} = \frac{100}{4189\ \times (18-8)} = 0.00239\ kg/s$$

1.2.2 Calculate Reynolds number:

Reynolds number is defined by

$$Re = \frac{inertial\ forces}{viscous\ forces} = \frac{D_h v \rho}{\mu} \tag{5}$$

Where
D_h = the inside hydraulic diameter of the pipe,
v =the average velocity of the fluid,
ρ =the density of the fluid,
μ = dynamic viscosity of the liquid which can be found in Appendix D.
It is common to use the mass flow rate $\dot{m}$ instead of the average velocity. The mass flow rate is related to the volumetric flow rate, $\dot{m} = \rho \dot{V}$, and we can write $\dot{V} = \frac{\pi}{4} {D_h}^2 v$. Therefore, the Reynolds number also can be defined as:

$$Re = \frac{4\dot{m}}{\pi D_h \mu} \tag{6}$$

Throughout the length of the tube, the mass flow rate is assumed to be constant.
For a circular tube, the hydraulic diameter is simply the diameter of the tube. Specifically,

Appendix C: Design calculations

D_{hr}= 9.53 - 2 × 0.57 =8.39 mm,

D_{hw}= (15.88-2 × 0.71) - 9.53 =4.93 mm,

$\mu_{er} = 2.947 \times 10^{-4}$ kg/m · s (Saturated liquid state at average temperature of -5 ℃),

$\mu_{ew} = 1.21 \times 10^{-3}$ kg/m · s (Saturated liquid state at average temperature of 13 ℃).

Therefore,

$$Re_r = \frac{4\dot{m}_{er}}{\pi D_{hr}\mu_{er}} = \frac{4 \times 0.00057}{\pi \times 0.00839 \times 2.947 \times 10^{-4}} = 294$$

$$\mathrm{Re_w} = \frac{4\dot{m}_{ew}}{\pi D_{hw}\mu_{ew}} = \frac{4 \times 0.00239}{\pi \times 0.00493 \times 1.21 \times 10^{-3}} = 510.4$$

The Reynolds number provides convenient criteria for distinguishing the flow regime in the pipes, which is critical to analyse the convection heat transfer problems. Values depend on the surface roughness of the pipe and the velocity fluctuations in the flow. It is generally accepted that [42]:

$Re < 2300$, laminar flow

$2300 < Re < 4000$, transition to turbulence

$Re > 4000$, turbulent flow

So both the refrigerant liquid and the coolant are laminar flow.

1.2.3 Estimate overall heat transfer coefficient

For fully developed laminar flow with constant heat flux, Nusselt number is constant value of 4.36 [42]. Find thermal conductivity from Appendix D, k_{er}=0.0968 $W/m \cdot K$; k_{ew}=0.585 $W/m \cdot K$

Since

$$Nu = \frac{h_i \times D_h}{k} \tag{7}$$

The following relationship is used to calculate the heat transfer coefficient:

$$h_i = \frac{Nu \times k_r}{D_h} \tag{8}$$

$$h_{ei} = \frac{Nu \times k_{er}}{D_{hr}} = \frac{4.36 \times 0.0968}{0.00839} \approx 50.3\ W/m^2 \cdot K$$

$$h_{eo} = \frac{Nu \times k_{ew}}{D_{hw}} = \frac{4.36 \times 0.585}{0.00493} \approx 517\ W/m^2 \cdot K$$

Appendix C: Design calculations

Except of the Equation (4), the heat transfer rate across a heat exchanger is usually expressed in the form:

$$\dot{Q} = UA\Delta T \tag{9}$$

Where

$\dot{Q}$=heat transfer rate,
U = overall heat transfer coefficient,
A= heat transfer surface area.

$$A = \pi DL \tag{10}$$

ΔT= logarithmic mean temperature difference (K);

From

$$\dot{Q} = \frac{\Delta T}{R} = UA\Delta T \tag{11}$$

We have:

$$R = \frac{1}{UA} \tag{12}$$

The total thermal Resistance becomes

$$\mathrm{R} = R_i + R_{wall} + R_o = \frac{1}{h_i A_i} + \frac{ln\frac{D_o}{D_i}}{2\pi kL} + \frac{1}{h_o A_o} \tag{13}$$

As when the wall thickness of the pipe is small and the thermal conductivity of the pipe material is high, as is usually the case, the thermal resistance of the pipe is negligible ($R_{wall} \approx 0$) the Equation (12) for the overall heat transfer coefficient simplifies to:

$$\frac{1}{UA} = R \approx \frac{1}{h_i A_i} + \frac{1}{h_o A_o} \tag{14}$$

The smaller heat transfer coefficient creates a bottleneck on the path of heat flow and seriously impedes heat transfer. This situation arises frequently when one of the fluids is a gas and the other is a liquid. Also, phase-processes involve very high heat transfer coefficients. To enhance the heat transfer on the gas side, we estimate $\mathrm{U} \approx \mathrm{h}_o$. And given the inner and outer surfaces of the pipe are almost identical ($A_i \approx A_o \approx A$), therefore:

$$\frac{1}{U_e} \approx \frac{1}{h_o} = \frac{1}{517}$$

Appendix C: Design calculations

1.2.4 Confirm the length

From equation (9) and (10), we have

$$L = \frac{\dot{Q}}{U \times \pi \times D \times \Delta T} \tag{15}$$

Logarithmic mean temperature difference follows the equation:

$$\Delta T = \frac{\Delta T_1 - \Delta T_2}{ln\frac{\Delta T_1}{\Delta T_2}} \tag{16}$$

Where

ΔT_1 = the temperature difference between the two fluids at end 1,

ΔT_2 = the temperature difference between the two fluids at end 2.

$$\therefore \Delta T_e = \frac{[18-(-5)]-[8-(-5)]}{ln\frac{23}{13}} \approx 17.5\ ℃$$

$$L_e = \frac{100}{517 \times \pi \times 9.53 \times 10^{-3} \times 17.5} \approx 369\ m\text{m}$$

Appendix C: Design calculations

2. CONDENSER:

Likewise, by assuming:

$$\dot{m}_{cr} = \dot{m}_{er} = 0.00057\ kg/s$$

$$\dot{m}_{cw} = \dot{m}_{ew} = 0.00239\ kg/s$$

The dimension of the condenser is estimated by separating it into two parts, which is:
The process from superheated vapour to saturated vapour, and the process from the saturated vapour to saturated liquid.

2.1 The length from saturated vapour to saturated liquid state.

2.1.1 Calculate the Reynolds number

Find the refrigerant's dynamic viscosity values from Appendix D:
$1.408 \times 10^{-5}\ kg/m \cdot s$ is the R134a's dynamic viscosity value at saturated vapour state with temperature of 40 ℃, $1.660 \times 10^{-4}\ kg/m \cdot s$ is the R134a's dynamic viscosity value at saturated liquid state with temperature of 40 ℃. The mean value, $\bar{\mu} = \frac{1.408\times10^{-5}+1.660\times10^{-4}}{2} = 9 \times 10^{-5}\ kg/m \cdot s$ is taken and substituted to the Reynolds Equation (6):

$$Re_{cr} = \frac{4 \times 0.00057}{9 \times 10^{-5} \times \pi \times 0.00839} \approx 961.7$$

2.1.2 Estimate the overall heat transfer coefficent:

The heat released from saturated vapour to saturated liquid state $\Delta h_{c2} = h_{st} - h_3$, h_{st} is the enthalpy of the saturated vapour refrigerant at 40 ℃.

From equation (2), heat released from condenser:

$$\dot{Q}_{c2} = \dot{m}_{cr} \times \Delta h_{c2} = 0.00057 \times (322 - 158) = 93.5\ W$$

Steady state condition is required, so the heat from the water:

$$\dot{Q}_{cw} = \dot{m}_{cw} \times C_w \times \Delta T_w \tag{17}$$

$$93.5 = 0.00239 \times C_w \times (T_c - 18)$$

By assuming the $C_w = 4.189$, estimate the coolant temperature at the middle state of T_{cm}:

$$(T_{cm} - 18) = \frac{93.5}{0.00239 \times 4189} = 9.3\ ℃$$

Therefore, $T_{cm} = 9.3 + 18 = 27.3$ ℃.
The estimated value of $4189\ J/kg.K$ can be re-checked by interpolation calculate the C_w from appendix D, and resulted in the same $T_{cm} = 27.3$ ℃.

Appendix C: Design calculations

Therefore, $\mu_{cw} = 0.937 \times 10^{-3}\ kg/m \cdot s$ (Saturated liquid state at average temperature of 22.7 ℃).

$$Re_{cw} = \frac{4\dot{m}_{cw}}{\pi D_{hw}\mu_{cw}} = \frac{4 \times 0.00239}{\pi \times 0.00493 \times 0.937 \times 10^{-3}} \approx 659$$

For laminar flow, it can be confirmed that, $Nu_c = 4.36$.
Find thermal conductivity from Appendix D:
k_{cr}=$\frac{0.0161+0.0757}{2} = 0.0459\ W/m \cdot K$, k_{cw}=0.603 $W/m \cdot K$. And substitute to Equation (8):

$$h_{ci} = \frac{Nu_{cr} \times k_{cr}}{D_{hr}} = \frac{4.36 \times 0.0459}{0.00839} \approx 23.85\ W/m^2 \cdot K$$
$$h_{co} = \frac{Nu_{cw} \times k_{cw}}{D_{hw}} = \frac{4.36 \times 0.603}{0.00493} \approx 533.3\ W/m^2 \cdot K$$
$$\therefore \frac{1}{U_c} \approx \frac{1}{h_{co}} = \frac{1}{533.3}$$

2.1.3 Confirm the length:

$$\Delta T_{c2} = \frac{(40 - 27.3) - (40 - 18)}{ln\frac{12.7}{22}} \approx 16.9$$

From equation (15):

$$L_{c2} = \frac{93.5}{533.3 \times \pi \times 9.53 \times 10^{-3} \times 16.9} \approx 347\ mm$$

2.2 The length from superheated vapour to saturate vapour state.

2.2.1 Calculate the Reynolds number

Find the refrigerant's dynamic viscosity values from Appendix D:

$1.408 \times 10^{-5}\ kg/m \cdot s$, and $2.187 \times 10^{-5}\ kg/m \cdot s$ are the R134a's dynamic viscosity value at saturated vapour state with temperatures of 40 ℃ and 90 ℃ respectively. We estimate the $\bar{\mu} = \frac{1.408\times10^{-5}+2.187\times10^{-5}}{2} = 1.8 \times 10^{-5}\ kg/m \cdot s$, and substitute the values to Equation (6):

$$Re_{cr} = \frac{4\times0.00057}{1.8\times10^{-5}\times\pi\times0.00839} \approx 4808.5 \text{ (Turbulent flow)}$$

2.2.2 Calculate the Prandtl number

$$Pr = \frac{viscous\ diffusion\ rate}{thermal\ diffusion\ rate} = \frac{C_p\mu}{k} \quad (18)$$

Where

Appendix C: Design calculations

μ = dynamic viscosity ($kg/m \cdot s$),
k = thermal conductivity ($W/m \cdot K$),
C_p = specific heat ($J/kg \cdot K$).
Find the mean values of the refrigerant parameters from Appendix D.

($\overline{C_p} = \frac{1138+2701}{2} = 1919.5\, J/kg \cdot K, \bar{k} = \frac{0.01610+0.02357}{2} = 0.0198\, W/m \cdot K$), and substitute to Equation (18),

$$\therefore Pr_{c1} = \frac{1919.5 \times 1.8 \times 10^{-5}}{0.0198} \approx 1.745$$

2.2.3 Calculate Nusselt number

For turbulent flow, Gnielinski correlation is used to reduce errors of the Nusselt number for $0.5 \leq \text{Pr} \leq 2000$, and $3000 \leq \text{Re} \leq 5 \times 10^6$.

$$Nu = \frac{(\frac{f}{8})(Re - 1000)Pr}{1 + 12.7\left(\frac{f}{8}\right)^{\frac{1}{2}}(Pr^{\frac{2}{3}} - 1)} \tag{19}$$

Where, friction factor

$$f = (0.790lnRe - 1.64)^{-2} \qquad 3000 \leq Re \leq 5 \times 10^6 \tag{20}$$

$$\therefore f_{cr1} = (0.790\ln Re_{cr} - 1.64)^{-2} \approx 0.039$$

Substitute the values of Prandtl number and the friction factor to Equation (19)

$$Nu_{c1} = \frac{(\frac{0.039}{8}) \times (4808.5 - 1000) \times 1.745}{1 + 12.7\left(\frac{0.039}{8}\right)^{\frac{1}{2}}(1.745^{\frac{2}{3}} - 1)} \approx 23.2$$

2.2.4 Estimate overall heat transfer coefficient

The heat released from the superheated vapour to the saturated vapour state $\Delta h_{c1} = h_2 - h_c$, From equation (2), heat released from this part of the condenser:

$$\dot{Q}_{c1} = \dot{m}_{cr} \times \Delta h_{c1} = 0.00057 \times (375 - 322) = 53\, W$$

Estimate the outlet temperature of the cooling water:

From Equation (4):

$$53 = 0.00239 \times C_w \times (T_{cwo} - 27.3)$$

By assuming the $C_w = 4.189\ kJ/kg.K$, estimate the coolant temperature at the outlet:

$$T_{cwo\prime} = \frac{53}{0.00239 \times 4189} + 27.3 \approx 32.6\,℃$$

Appendix C: Design calculations

As mentioned in the previous section. The estimated value of $4189\ J/kg.K$ can be re-checked by interpolation calculate the C_w from appendix D, and resulted in the same $T_{cwo} = 32.6$ ℃.
Therefore, $\mu_{cw1} = 0.798 \times 10^{-3}\ kg/m \cdot s$ (Saturated liquid state at average temperature of 30 ℃);

$$Re_{cw1} = \frac{4\dot{m}_{cw}}{\pi D_{hw}\mu_{cw1}} = \frac{4 \times 0.00239}{\pi \times 0.00493 \times 0.798 \times 10^{-3}} \approx 774$$

For laminar flow, it can be confirmed that, $N_{uc} = 4.36$.
Find thermal conductivity from Appendix D,

k_{cr1}=$\frac{0.0161+0.0757}{2} = 0.0459\ W/m \cdot K$; k_{cw1}=0.615 $W/m \cdot K$; Substitute the values to the Equation (8):

$$h_{ci} = \frac{Nu_{cr1} \times k_{cr1}}{D_{hr}} = \frac{23.2 \times 0.0198}{0.00839} \approx 54.75\ W/m^2 \cdot K$$
$$h_{co} = \frac{Nu_{cw} \times k_{cw1}}{D_{hw}} = \frac{4.36 \times 0.615}{0.00493} \approx 543.9\ W/m^2 \cdot K$$
$$U_{c1} \approx h_{co1} = 543.9\ W/m^2 \cdot K$$

2.2.5 Confirm the length

$$\Delta T_{c1} = \frac{(90 - 32.6) - (40 - 27.3)}{ln\frac{57.4}{12.7}} \approx 29.8$$

From equation (15):

$$L_{c1} = \frac{53}{543.9 \times \pi \times 9.53 \times 10^{-3} \times 29.8} \approx 109\ mm$$

$$\therefore L_c = L_{c1} + L_{c2} = 347 + 109 = 456\ mm$$

Appendix C: Design calculations

3. PRE-COOLER:

The heat exchanger design is an iterative process. Likewise,

$$\dot{Q}_{pc} = \dot{m}_r \times \Delta h_{pc} = 0.00057 \times 35 \approx 20\ W$$

$U_0 \approx 350\ W/m^2.℃$ was estimated from empirical approximation table[23].

Assuming the temperature conditions of the evaporator as shown in Figure C-1.

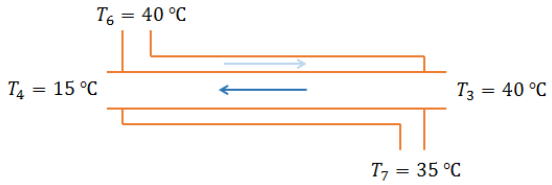

Figure C-1. Temperature condition at the pre-cooler

$$\Delta T_{mpc1} = 40 - 35 = 5, \qquad \Delta T_{mpc2} = 15 - (-5) = 20$$

$$\Delta T_{mpc} = 11\ ℃$$

$$L_{pc} = \frac{20}{350 \times \pi \times 9.53 \times 11} \times 10^3 \approx 174\ mm$$

Appendix C: Design calculations

4. GENERATOR:

For the conditions in the absorber, the heat exchanger, and the generator. The mixture of R134a and TEG.DME is involved. Therefore, the previous method using the pure liquid properties is not applicable.

The h-x diagram in Figure C-2 depicts the enthalpy of the mixture as a function of the weight fraction of the refrigerant based on correlations between the pressure, temperature and weight fraction in the state of equilibrium. By assuming the given heat is 120 ℃,

$h_g = 165\ \text{kcal/kg} = 689\ \text{kJ/kg}$;

$x^{st} = 0.25$ kg/kg (The concentration of the strong solution at the boiler).

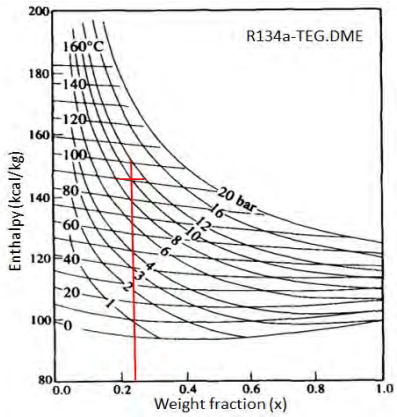

Figure C-2. Redrawn Enthalpy-Concentration diagram of the mixture of R134a-TEG.DME from Borde[11].

From Vicatos[50] approach, the generator receives strong solution with concentration x^{st} with the mass flow rate of f kg, so that 1kg of vapour with concentration y is released. At the same time (f-1) kg/kg weak solution with concentration x^{we} is returned to the absorber. f is the rate of relative circulation.

$$\frac{1}{f-1} = \frac{x^{st} - x^{we}}{y - x^{st}} \tag{21}$$

The equation (21) is from Figure C-3, which was initially developed from an ammonia absorption system. If a unit length is assigned to the length ($x^{st} - x^{we}$). From the similar triangles 8-K-A and 10-L-A, it can be observed that the ratio (8-10):(10-A) represents the ratio of the mass flow rates of the vapour to the weak solution. That is, 1:(f-1).

$$f = \frac{y - x^{we}}{x^{st} - x^{we}} \tag{22}$$

In our case, y=1 kg/kg, $x^{we} = 0$ (pure TEG.DME., ideally), $x^{st} = 0.25\ kg/kg$,

$$\therefore f = 4$$

Appendix C: Design calculations

$$\dot{m}_{str} = f \times \dot{m}_r = 4 \times 0.00057 = 0.00228\ kg/s$$

$$\dot{m}_{we} = (f-1) \times \dot{m}_r = (4-1) \times 0.00057 = 0.00171\, kg/s$$

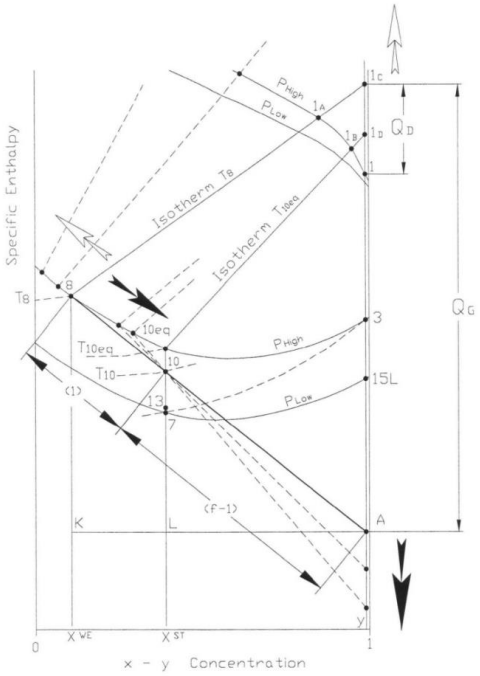

Figure C-3: Source: Picture courtesy of G. Vicatos [50]

A reasonable choice of 200 mm length heating element was selected among the available options, shorter ones can lead risk of liquid damaging due to its high heat transfer. The boiler height was then determined to be 220 mm.

5. SEPARATOR:

From the analysis of the bubble pump, separator parameters such as the diameter and the length are not critical. It was eventually designed to be $5/8''$ (15.88 mm) in diameter, 140 mm length, which is able to allow 60 mm immersed lifting section.

Appendix C: Design calculations

6. ABSORBER:

A heat balance of the system gives:

$$\dot{Q}_g + \dot{Q}_e = \dot{Q}_c + \dot{Q}_{pc} + \dot{Q}_a \quad (23)$$

$$689 \times 0.00228 + 175 \times 0.00057 = (217 + 35) \times 0.00057 + \Delta h_a \times 0.00171$$

Δh_a= 893 kJ/kg

$$\dot{Q}_a = \dot{m}_{we} \times \Delta h_a = 0.00171 \times 893 \approx 1527\ W$$

By estimating:

$\Delta T_{a1} = 80 - 28 = 52$ ℃

$\Delta T_{a2} = 40 - 18 = 22$ ℃

$$\Delta T_{ma} = \frac{\Delta T_{a1} - \Delta T_{a2}}{ln\frac{\Delta T_{a1}}{\Delta T_{a2}}} \approx 35\ ℃$$

At an average temperature of 23 ℃

$k_{aw} = 0.0842\ W/m \cdot K$

$\mu_{aw} = 2.064 \times 10^{-4}\ kg/m \cdot s$

$$R_{aw} = \frac{4\dot{m}_w}{\pi D_{hw}\mu_{aw}} = \frac{4 \times 0.00239}{\pi \times 0.00473 \times 2.064 \times 10^{-4}} = 3119$$

From Equation (20)

$$f_a = (0.790 ln R_e - 1.64)^{-2} = 0.045$$

Find the mean values from Appendix D.

$\overline{C_{pa}} = \frac{1401+1440}{2} = 1420.5\ J/kg \cdot K,$

$\overline{k_a} = \frac{0.0860+0.0818}{2} = 0.0839\ W/m \cdot K,$

$\bar{\mu}_a = \frac{2.197+1.938}{2} = 2.068 \times 10^{-4}\ kg/m \cdot s.$

Substitute to Equation (18):

$$\therefore Pr_a = \frac{1420.5 \times 2.068 \times 10^{-4}}{0.0839} \approx 3.5$$

Appendix C: Design calculations

$$Nu_a = \frac{(\frac{f}{8})(Re - 1000)Pr}{1 + 12.7\left(\frac{f}{8}\right)^{\frac{1}{2}}(P_r^{\frac{2}{3}} - 1)} \approx 18.63$$

$$\therefore U_{ao} = h_{ao} = \frac{Nu_a \times k_0}{d_h} \approx 330\ W/m^2 \cdot ℃$$

$$L_a \approx 618\ mm$$

Appendix C: Design calculations

7. HEAT EXCHANGER:

Figure C-4. Temperature condition at the solution heat exchanger

As confirmed: $\Delta h_a = 893$ kJ/kg = $h_{13} + h_7$, $h_{13} = \Delta h_a - h_7 = 893 - 333 = 560$ kJ/kg,
We have:

$$h_9 = h_2 = 375\ kJ/kg$$
$$h_{10} = h_{13} = 560\ kJ/kg$$

From

$$\dot{Q}_{ex} = (f-1) \times (h_9 - h_{10}) = f \times (h_{12} - h_{11}) \quad (24)$$

$$(4-1) \times (375 - 560) = 4 \times (h_{12} - 298)$$
$$h_{12} = 553\ kJ/kg$$
$$\Delta h_{ex} = (f-1) \times (h_9 - h_{10}) = 1020\ kJ/kg$$
$$\therefore \dot{Q}_{ex} = \dot{m}_{str} \times \Delta h_{ex} = 0.00228 \times 1020 = 2.3\ kW$$

7.1 For inner pipe (weak solution)

Applying the equation:

$$ln(\mu) = \mu_0 + \frac{\mu_1}{T + \mu_2} \quad (25)$$

This equation is obtained by regression using the Statistical Package for Social Sciences (SPSS) by Borde[11] in calculation of dynamic viscosity of R134a-TEG.DME mixture. Where μ is expressed in Centipoise and T in Kelvin, and for pure TEG.DME:
$\mu_0 = -3.157$, $\mu_1 = 844.54$, $\mu_2 = -103.2$.
At an average temperature of 85 ℃:

$$\mu_{exi} \approx 1.17\ cP = 1.17 \times 10^{-3}\ kg/m \cdot s$$
$$D_{hi} = 12.7 - 0.61 \times 2 = 11.48\ mm$$

$$Re_{xi} = \frac{4\dot{m}_{st}}{\pi D_{hexi} \mu_{exi}} = \frac{4 \times 0.00171}{\pi \times 0.01148 \times 1.17 \times 10^{-3}} = 172\ (laminar\ flow)$$

Appendix C: Design calculations

7.2 For outer pipe (strong solution)

At an average temperature of 55 ℃, the dynamic viscosity of the R134a-TEG.DME mixture was estimated from the Figure$\mu_{exo} \approx 1.8 \times 10^{-3}\ \mathrm{kg/m \cdot s}$

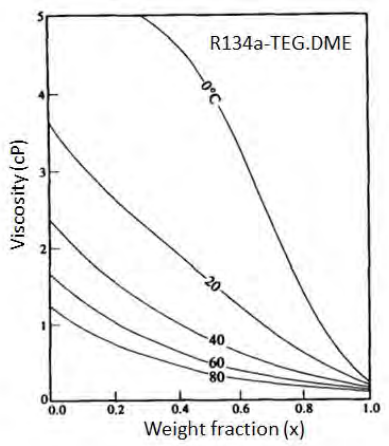

Figure C-5. Redrawn Cp-x diagram of the mixture of R134a-TEG.DME from Borde[11].

$$Re_{xo} = \frac{4 \times 0.00228}{\pi \times 0.00538 \times 1.8 \times 10^{-3}} \approx 300\ (laminar\ flow)$$

Applying the Equation (15):

$$\Delta T_m = \frac{\Delta T_1 - \Delta T_2}{ln\left(\frac{\Delta T_1}{\Delta T_2}\right)} = \frac{20 - 40}{ln\left(\frac{20}{40}\right)} \approx 29\ ℃$$

$$L_{ex} = \frac{2300}{3500 \times \pi \times 11.48 \times 10^{-3} \times 29} \approx 629\ mm$$

Appendix D: Property tables of saturated water and R134a

Properties of saturated water

Temp. T, °C	Saturation Pressure P_{sat}, kPa	Density ρ, kg/m³ Liquid	Density ρ, kg/m³ Vapor	Enthalpy of Vaporization h_{fg}, kJ/kg	Specific Heat c_p, J/kg·K Liquid	Specific Heat c_p, J/kg·K Vapor	Thermal Conductivity k, W/m·K Liquid	Thermal Conductivity k, W/m·K Vapor	Dynamic Viscosity μ, kg/m·s Liquid	Dynamic Viscosity μ, kg/m·s Vapor	Prandtl Number Pr Liquid	Prandtl Number Pr Vapor	Volume Expansion Coefficient β, 1/K Liquid
0.01	0.6113	999.8	0.0048	2501	4217	1854	0.561	0.0171	1.792×10^{-3}	0.922×10^{-5}	13.5	1.00	-0.068×10^{-3}
5	0.8721	999.9	0.0068	2490	4205	1857	0.571	0.0173	1.519×10^{-3}	0.934×10^{-5}	11.2	1.00	0.015×10^{-3}
10	1.2276	999.7	0.0094	2478	4194	1862	0.580	0.0176	1.307×10^{-3}	0.946×10^{-5}	9.45	1.00	0.733×10^{-3}
15	1.7051	999.1	0.0128	2466	4185	1863	0.589	0.0179	1.138×10^{-3}	0.959×10^{-5}	8.09	1.00	0.138×10^{-3}
20	2.339	998.0	0.0173	2454	4182	1867	0.598	0.0182	1.002×10^{-3}	0.973×10^{-5}	7.01	1.00	0.195×10^{-3}
25	3.169	997.0	0.0231	2442	4180	1870	0.607	0.0186	0.891×10^{-3}	0.987×10^{-5}	6.14	1.00	0.247×10^{-3}
30	4.246	996.0	0.0304	2431	4178	1875	0.615	0.0189	0.798×10^{-3}	1.001×10^{-5}	5.42	1.00	0.294×10^{-3}
35	5.628	994.0	0.0397	2419	4178	1880	0.623	0.0192	0.720×10^{-3}	1.016×10^{-5}	4.83	1.00	0.337×10^{-3}
40	7.384	992.1	0.0512	2407	4179	1885	0.631	0.0196	0.653×10^{-3}	1.031×10^{-5}	4.32	1.00	0.377×10^{-3}
45	9.593	990.1	0.0655	2395	4180	1892	0.637	0.0200	0.596×10^{-3}	1.046×10^{-5}	3.91	1.00	0.415×10^{-3}
50	12.35	988.1	0.0831	2383	4181	1900	0.644	0.0204	0.547×10^{-3}	1.062×10^{-5}	3.55	1.00	0.451×10^{-3}
55	15.76	985.2	0.1045	2371	4183	1908	0.649	0.0208	0.504×10^{-3}	1.077×10^{-5}	3.25	1.00	0.484×10^{-3}
60	19.94	983.3	0.1304	2359	4185	1916	0.654	0.0212	0.467×10^{-3}	1.093×10^{-5}	2.99	1.00	0.517×10^{-3}
65	25.03	980.4	0.1614	2346	4187	1926	0.659	0.0216	0.433×10^{-3}	1.110×10^{-5}	2.75	1.00	0.548×10^{-3}
70	31.19	977.5	0.1983	2334	4190	1936	0.663	0.0221	0.404×10^{-3}	1.126×10^{-5}	2.55	1.00	0.578×10^{-3}
75	38.58	974.7	0.2421	2321	4193	1948	0.667	0.0225	0.378×10^{-3}	1.142×10^{-5}	2.38	1.00	0.607×10^{-3}
80	47.39	971.8	0.2935	2309	4197	1962	0.670	0.0230	0.355×10^{-3}	1.159×10^{-5}	2.22	1.00	0.653×10^{-3}
85	57.83	968.1	0.3536	2296	4201	1977	0.673	0.0235	0.333×10^{-3}	1.176×10^{-5}	2.08	1.00	0.670×10^{-3}
90	70.14	965.3	0.4235	2283	4206	1993	0.675	0.0240	0.315×10^{-3}	1.193×10^{-5}	1.96	1.00	0.702×10^{-3}
95	84.55	961.5	0.5045	2270	4212	2010	0.677	0.0246	0.297×10^{-3}	1.210×10^{-5}	1.85	1.00	0.716×10^{-3}
100	101.33	957.9	0.5978	2257	4217	2029	0.679	0.0251	0.282×10^{-3}	1.227×10^{-5}	1.75	1.00	0.750×10^{-3}
110	143.27	950.6	0.8263	2230	4229	2071	0.682	0.0262	0.255×10^{-3}	1.261×10^{-5}	1.58	1.00	0.798×10^{-3}
120	198.53	943.4	1.121	2203	4244	2120	0.683	0.0275	0.232×10^{-3}	1.296×10^{-5}	1.44	1.00	0.858×10^{-3}
130	270.1	934.6	1.496	2174	4263	2177	0.684	0.0288	0.213×10^{-3}	1.330×10^{-5}	1.33	1.01	0.913×10^{-3}
140	361.3	921.7	1.965	2145	4286	2244	0.683	0.0301	0.197×10^{-3}	1.365×10^{-5}	1.24	1.02	0.970×10^{-3}
150	475.8	916.6	2.546	2114	4311	2314	0.682	0.0316	0.183×10^{-3}	1.399×10^{-5}	1.16	1.02	1.025×10^{-3}
160	617.8	907.4	3.256	2083	4340	2420	0.680	0.0331	0.170×10^{-3}	1.434×10^{-5}	1.09	1.05	1.145×10^{-3}
170	791.7	897.7	4.119	2050	4370	2490	0.677	0.0347	0.160×10^{-3}	1.468×10^{-5}	1.03	1.05	1.178×10^{-3}
180	1,002.1	887.3	5.153	2015	4410	2590	0.673	0.0364	0.150×10^{-3}	1.502×10^{-5}	0.983	1.07	1.210×10^{-3}
190	1,254.4	876.4	6.388	1979	4460	2710	0.669	0.0382	0.142×10^{-3}	1.537×10^{-5}	0.947	1.09	1.280×10^{-3}
200	1,553.8	864.3	7.852	1941	4500	2840	0.663	0.0401	0.134×10^{-3}	1.571×10^{-5}	0.910	1.11	1.350×10^{-3}
220	2,318	840.3	11.60	1859	4610	3110	0.650	0.0442	0.122×10^{-3}	1.641×10^{-5}	0.865	1.15	1.520×10^{-3}
240	3,344	813.7	16.73	1767	4760	3520	0.632	0.0487	0.111×10^{-3}	1.712×10^{-5}	0.836	1.24	1.720×10^{-3}
260	4,688	783.7	23.69	1663	4970	4070	0.609	0.0540	0.102×10^{-3}	1.788×10^{-5}	0.832	1.35	2.000×10^{-3}
280	6,412	750.8	33.15	1544	5280	4835	0.581	0.0605	0.094×10^{-3}	1.870×10^{-5}	0.854	1.49	2.380×10^{-3}
300	8,581	713.8	46.15	1405	5750	5980	0.548	0.0695	0.086×10^{-3}	1.965×10^{-5}	0.902	1.69	2.950×10^{-3}
320	11,274	667.1	64.57	1239	6540	7900	0.509	0.0836	0.078×10^{-3}	2.084×10^{-5}	1.00	1.97	
340	14,586	610.5	92.62	1028	8240	11,870	0.469	0.110	0.070×10^{-3}	2.255×10^{-5}	1.23	2.43	
360	18,651	528.3	144.0	720	14,690	25,800	0.427	0.178	0.060×10^{-3}	2.571×10^{-5}	2.06	3.73	
374.14	22,090	317.0	317.0	0	—	—	—	—	0.043×10^{-3}	4.313×10^{-5}			

Note 1: Kinematic viscosity ν and thermal diffusivity α can be calculated from their definitions, $\nu = \mu/\rho$ and $\alpha = k/\rho c_p = \nu/\text{Pr}$. The temperatures 0.01°C, 100°C, and 374.14°C are the triple-, boiling-, and critical-point temperatures of water, respectively. The properties listed above (except the vapor density) can be used at any pressure with negligible error except at temperatures near the critical-point value.

Note 2: The unit kJ/kg·°C for specific heat is equivalent to kJ/kg·K, and the unit W/m·°C for thermal conductivity is equivalent to W/m·K.

Source: Viscosity and thermal conductivity data are from J. V. Sengers and J. T. R. Watson, *Journal of Physical and Chemical Reference Data* 15 (1986), pp. 1291–1322. Other data are obtained from various sources or calculated.

Appendix D: Property tables of saturated water and R134a

Properties of saturated refrigerant–134a

Temp. T, °C	Saturation Pressure P, kPa	Density ρ, kg/m³ Liquid	Density ρ, kg/m³ Vapor	Enthalpy of Vaporization h_{fg}, kJ/kg	Specific Heat c_p, J/kg·K Liquid	Specific Heat c_p, J/kg·K Vapor	Thermal Conductivity k, W/m·K Liquid	Thermal Conductivity k, W/m·K Vapor	Dynamic Viscosity μ, kg/m·s Liquid	Dynamic Viscosity μ, kg/m·s Vapor	Prandtl Number Pr Liquid	Prandtl Number Pr Vapor	Volume Expansion Coefficient β, 1/K Liquid	Surface Tension, N/m
−40	51.2	1418	2.773	225.9	1254	748.6	0.1101	0.00811	4.878×10^{-4}	2.550×10^{-6}	5.558	0.235	0.00205	0.01760
−35	66.2	1403	3.524	222.7	1264	764.1	0.1084	0.00862	4.509×10^{-4}	3.003×10^{-6}	5.257	0.266	0.00209	0.01682
−30	84.4	1389	4.429	219.5	1273	780.2	0.1066	0.00913	4.178×10^{-4}	3.504×10^{-6}	4.992	0.299	0.00215	0.01604
−25	106.5	1374	5.509	216.3	1283	797.2	0.1047	0.00963	3.882×10^{-4}	4.054×10^{-6}	4.757	0.335	0.00220	0.01527
−20	132.8	1359	6.787	213.0	1294	814.9	0.1028	0.01013	3.614×10^{-4}	4.651×10^{-6}	4.548	0.374	0.00227	0.01451
−15	164.0	1343	8.288	209.5	1306	833.5	0.1009	0.01063	3.371×10^{-4}	5.295×10^{-6}	4.363	0.415	0.00233	0.01376
−10	200.7	1327	10.04	206.0	1318	853.1	0.0989	0.01112	3.150×10^{-4}	5.982×10^{-6}	4.198	0.459	0.00241	0.01302
−5	243.5	1311	12.07	202.4	1330	873.8	0.0968	0.01161	2.947×10^{-4}	6.709×10^{-6}	4.051	0.505	0.00249	0.01229
0	293.0	1295	14.42	198.7	1344	895.6	0.0947	0.01210	2.761×10^{-4}	7.471×10^{-6}	3.919	0.553	0.00258	0.01156
5	349.9	1278	17.12	194.8	1358	918.7	0.0925	0.01259	2.589×10^{-4}	8.264×10^{-6}	3.802	0.603	0.00269	0.01084
10	414.9	1261	20.22	190.8	1374	943.2	0.0903	0.01308	2.430×10^{-4}	9.081×10^{-6}	3.697	0.655	0.00280	0.01014
15	488.7	1244	23.75	186.6	1390	969.4	0.0880	0.01357	2.281×10^{-4}	9.915×10^{-6}	3.604	0.708	0.00293	0.00944
20	572.1	1226	27.77	182.3	1408	997.6	0.0856	0.01406	2.142×10^{-4}	1.075×10^{-5}	3.521	0.763	0.00307	0.00876
25	665.8	1207	32.34	177.8	1427	1028	0.0833	0.01456	2.012×10^{-4}	1.160×10^{-5}	3.448	0.819	0.00324	0.00808
30	770.6	1188	37.53	173.1	1448	1061	0.0808	0.01507	1.888×10^{-4}	1.244×10^{-5}	3.383	0.877	0.00342	0.00742
35	887.5	1168	43.41	168.2	1471	1098	0.0783	0.01558	1.772×10^{-4}	1.327×10^{-5}	3.328	0.935	0.00364	0.00677
40	1017.1	1147	50.08	163.0	1498	1138	0.0757	0.01610	1.660×10^{-4}	1.408×10^{-5}	3.285	0.995	0.00390	0.00613
45	1160.5	1125	57.66	157.6	1529	1184	0.0731	0.01664	1.554×10^{-4}	1.486×10^{-5}	3.253	1.058	0.00420	0.00550
50	1318.6	1102	66.27	151.8	1566	1237	0.0704	0.01720	1.453×10^{-4}	1.562×10^{-5}	3.231	1.123	0.00456	0.00489
55	1492.3	1078	76.11	145.7	1608	1298	0.0676	0.01777	1.355×10^{-4}	1.634×10^{-5}	3.223	1.193	0.00500	0.00429
60	1682.8	1053	87.38	139.1	1659	1372	0.0647	0.01838	1.260×10^{-4}	1.704×10^{-5}	3.229	1.272	0.00554	0.00372
65	1891.0	1026	100.4	132.1	1722	1462	0.0618	0.01902	1.167×10^{-4}	1.771×10^{-5}	3.255	1.362	0.00624	0.00315
70	2118.2	996.2	115.6	124.4	1801	1577	0.0587	0.01972	1.077×10^{-4}	1.839×10^{-5}	3.307	1.471	0.00716	0.00261
75	2365.8	964	133.6	115.9	1907	1731	0.0555	0.02048	9.891×10^{-5}	1.908×10^{-5}	3.400	1.612	0.00843	0.00209
80	2635.2	928.2	155.3	106.4	2056	1948	0.0521	0.02133	9.011×10^{-5}	1.982×10^{-5}	3.558	1.810	0.01031	0.00160
85	2928.2	887.1	182.3	95.4	2287	2281	0.0484	0.02233	8.124×10^{-5}	2.071×10^{-5}	3.837	2.116	0.01336	0.00114
90	3246.9	837.7	217.8	82.2	2701	2865	0.0444	0.02357	7.203×10^{-5}	2.187×10^{-5}	4.385	2.658	0.01911	0.00071
95	3594.1	772.5	269.3	64.9	3675	4144	0.0396	0.02544	6.190×10^{-5}	2.370×10^{-5}	5.746	3.862	0.03343	0.00033
100	3975.1	651.7	376.3	33.9	7959	8785	0.0322	0.02989	4.765×10^{-5}	2.833×10^{-5}	11.77	8.326	0.10047	0.00004

Note 1: Kinematic viscosity ν and thermal diffusivity α can be calculated from their definitions, $\nu = \mu/\rho$ and $\alpha = k/\rho c_p = \nu/\mathrm{Pr}$. The properties listed here (except the vapor density) can be used at any pressures with negligible error except at temperatures near the critical-point value.

Note 2: The unit kJ/kg·°C for specific heat is equivalent to kJ/kg·K, and the unit W/m·°C for thermal conductivity is equivalent to W/m·K.

Source: Data generated from the EES software developed by S. A. Klein and F. L. Alvarado. Original sources: R. Tillner-Roth and H. D. Baehr, "An International Standard Formulation for the Thermodynamic Properties of 1,1,1,2-Tetrafluoroethane (HFC-134a) for Temperatures from 170 K to 455 K and Pressures up to 70 MPa," *J. Phys. Chem. Ref. Data*, Vol. 23, No. 5, 1994; M.J. Assael, N. K. Dalaouti, A. A. Griva, and J. H. Dymond, "Viscosity and Thermal Conductivity of Halogenated Methane and Ethane Refrigerants," *IJR*, Vol. 22, pp. 525–535, 1999; NIST REFPROP 6 program (M. O. McLinden, S. A. Klein, E. W. Lemmon, and A. P. Peskin, Physical and Chemical Properties Division, National Institute of Standards and Technology, Boulder, CO 80303, 1995).

Appendix E: P-h diagram of R134a

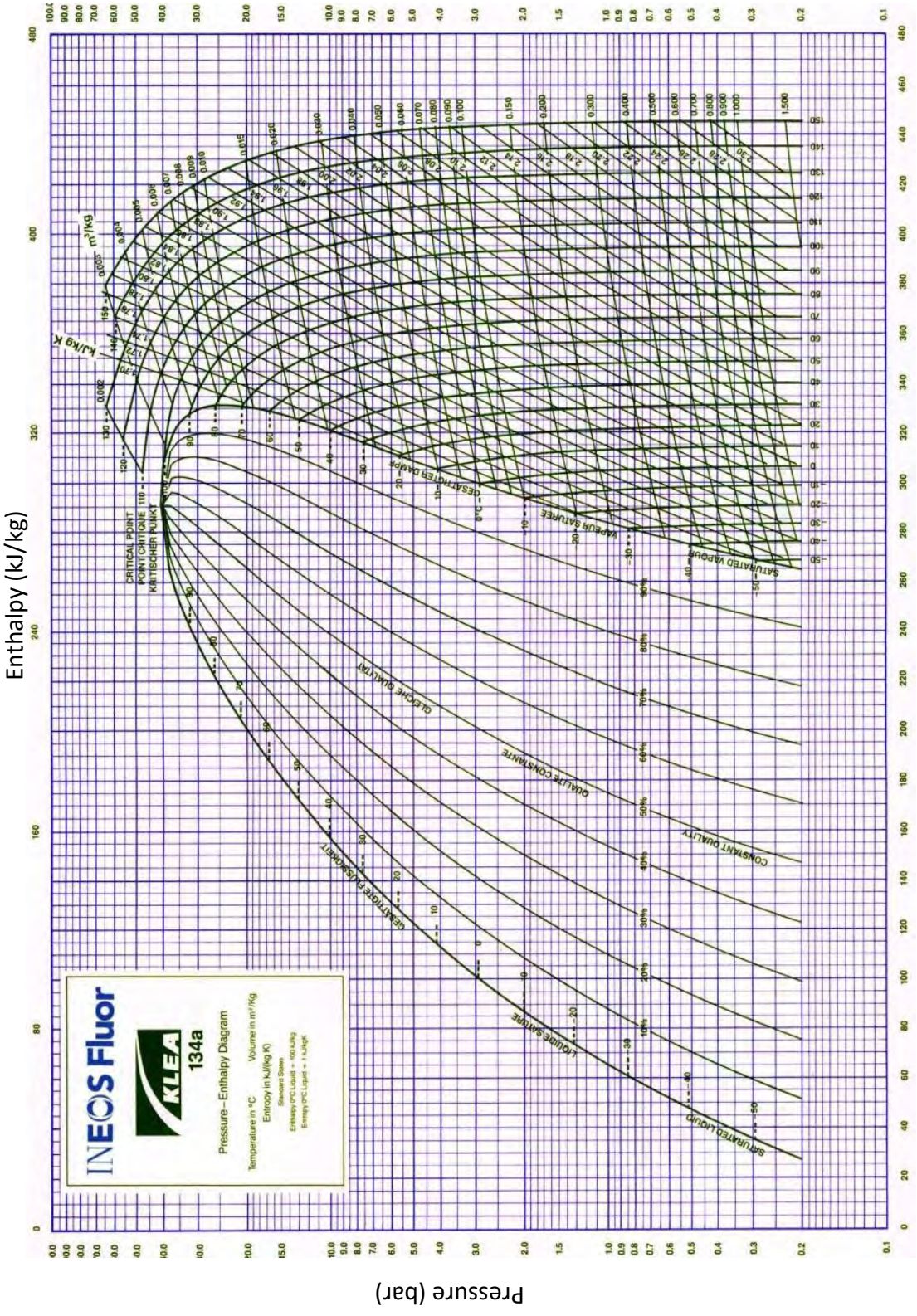

Appendix F: MATLAB code

```
%------------------------------Convert Gantner-------------------------------%

clear all;
tic

%% choose folder

folder = 'GAP_A13_Marina';
fprintf('Sample: %s\n', folder);

%% read experiments from files

% read general parameters from data file parameter.txt
fid = fopen(strcat(folder, '/parameter.txt'));

% read data
para = textscan(fid, '%f', 'CommentStyle','%');
fclose(fid);
para = cell2mat(para);

% save data into variables and convert to SI Units
V_1 = para(1)*10^-6;                % reservoir volume      [m^3]
V_2 = para(2)*10^-6;                % sample chamber volume [m^3]
V_gas = V_1+V_2;                    % total volume          [m^3]
m_ac = para(3)*10^-3;               % mass activated carbon [kg]

%% define constants

R = 8.3144621;                      % universal gas constant [J/mol/K]
MW = 32.04*10^-3;                   % molar mass of methanol [kg/mol]

%% create list of data with all files from data type ".csv" in "raw" folder

files = dir(strcat(folder,'/raw/*.csv'));
nfiles = numel(files);

for i = 1:nfiles                    % loop over all files

    % infile from raw folder - outfile in base folder, type csv
    infile  = strcat(folder,'/raw/',files(i).name);
    outfile = strcat(folder,'/',files(i).name);

    %% readout data

    % readout data without first two rows and columns (parameters name)
    data = dlmread(infile,',',2,2);

    % pressure - offset [mbar]
    p_met = data(:,1)-data(:,2);

    % temperatures [^\circC]
    tgas = data(:,3);               % T_1, temperature of sorption chamber
    tads = data(:,4);               % T_2, temperature of AC surface
```

Appendix F: MATLAB code

```
tcar = data(:,5);                % T_3, temperature of sample carrier
tamb = data(:,6);                % T_4, ambient temperature (lab)
thld = data(:,7);                % T_5, temperature of sample holder
                                  (PT100)

%% create outfile

% loop over all pressure values starting from the second value
for b=2:numel(p_met)

    % detect pressure drop
    if abs(p_met(b-1)-p_met(b)) >= 0.3

        % average values from before the pressure drop
        avg_p = mean(p_met(1:b-1));
        avg_tgas = mean(tgas(1:b-1));
        avg_tads  = mean(tads(1:b-1));
        avg_tcar  = mean(tcar(1:b-1));
        avg_tamb  = mean(tamb(1:b-1));
        avg_thld  = mean(thld(1:b-1));

        % Calculate theoretical pressure after the gas expanding from
          reservoir using Boyle-Mariotte's law:
         (In sample chamber using Boyle-Mariotte: p1/p2 = V_gas/V_1)
        p_0 = avg_p*V_1/V_gas;

        % open outfile and write header items
        fid = fopen(outfile, 'w');
        fprintf(fid,'Time,Pressure,T_Gas,T_Ads,T_Car,T_amb,T_Hld\n');
        fprintf(fid,'[s],[mbar],[ ^\circC],[ ^\circC],[ ^\circC],[
^\circC],
                [^\circC]\n');
        fclose(fid);

        % save first line with mean values at t0 = 0s
        t0 = [0 p_0 avg_tgas avg_tads avg_tcar avg_tamb avg_thld];
        dlmwrite(outfile,t0,'-append');

        break
    end
end

% loop over following data points
for b=b:numel(p_met)

   % check if pressure is lower than initial expanded pressure
   if p_met(b) < p_0

        % create time vector and matrix data2 with experimental data
        time = [0.1:0.1:size(p_met)/10-(b-1)/10]';
        data = [p_met data(:,3:7)];
```

Appendix F: MATLAB code

```
        % create matrix data3, time vector included
        data = [time data(b:end,:)];

        % export remaining data in .dat
        dlmwrite(outfile,data,'-append');
        break
    end
end

%% create structure with all important data

p_0 = p_0*100;                                % initial pressure [N/m^2]
p_eq = mean(data(end-20:end,2))*100;          % equilibrium pressure [N/m^2]

tads_eq = mean(data(end-20:end,4))+273.15; % equilibrium temperature of
                                              sample [K]
T_eq = tads_eq;                               % equilibrium temp [K]
T_0 = T_eq;                                   % initial temp (assumed to be
                                              equal as in eq.)


p_sat = p_sat_MeOH(T_eq)*10^5;                % vapour pressure MeOH [N/m^2]
rho_liq = rho_liq_MeOH(T_eq);                 % liquid density MeOH [kg/m^3]

buf = strsplit(files(i).name,'_');            % split string at delimiter '_'
buft = char(buf(2));
T_iso = sscanf(buft(2:end),'%f');             % write temperature from file-
                                              name in structure

%% general calculation of the adsorbed amount of substance
  (differentiation between adsorption, desorption and experiments in
   several steps)

if (strcmp(buf{4},'ads.csv') == 1)
        n_vl_0(i) = V_gas*p_0/(R*T_0);
        n_pk_0(i) = 0;
        n_ads_0(i)= 0;
end
if (strcmp(buf{4},'des.csv') == 1)
        n_vl_0(i) = 0;
        n_pk_0(i) = V_2*dat(i-1).p_eq/(R*dat(i-1).T_eq);
        n_ads_0(i)= n_fl_ads(i-1);
end
if (strcmp (buf{4},'stp') == 1)
      if (strcmp (buf{5},'1.csv') == 1)
          n_vl_0(i) = V_gas*p_0/(R*T_0);
          n_pk_0(i) = 0;
          n_ads_0(i)= 0;
      else
          n_vl_0(i) = V_gas*p_0/(R*T_0);
          n_pk_0(i)= V_gas*dat(i-1).p_eq/(R*dat(i-1).T_eq);
          n_ads_0(i)= n_fl_ads(i-1);
     end
end
```

Appendix F: MATLAB code

```
    n_ads(i)=n_vl_0(i)+n_pk_0(i)+n_ads_0(i)-(p_eq*V_gas/(R*T_eq));

    %% Calculate equilibrium data

    X_eq = n_ads(i)/m_ac*MW;                    % equilibrium loading [g/g]
    V_ads = n_ads(i) * MW / rho_liq;            % adsorbed volume [m^3]
    A_eq = R/MW*T_eq*log(p_sat/(p_eq))/1000;    % adsorption potential [J/g]
    W_eq = V_ads/m_ac*1000;                     % capacity [cm^3/g]


    %% write data in structures

    buft = char(buf(2));
    dat(i).T_iso = T_iso;      % write temperature from file-name in structure
    dat(i).name = files(i).name;
    dat(i).p_sat = p_sat;
    dat(i).rho_liq = rho_liq;
    dat(i).p_eq = p_eq;
    dat(i).T_eq = T_eq;
    dat(i).X_eq = X_eq;
    dat(i).A_eq = A_eq;
    dat(i).W_eq = W_eq;

    exp.A_eq(i)     = A_eq;    % adsorption potentials in a vector [J/g]
    exp.W_eq(i)     = W_eq;    % loadings in a vector [cm^3/g]
    exp.p_eq(i)     = p_eq;    % equilibrium pressure [Pa]
    exp.p_sat(i)    = p_sat;   % saturation pressure [Pa]
    exp.n           = nfiles;  % number of experiments
    exp.T_iso(i)    = T_iso;   % isothermal series temp (eg. 30 or 60 ^\circC)
    exp.fit(i)      = 1;       % flag if used for fitting (1) or not (0)
    exp.plot(i)     = 1;       % flag if used for plotting (1) or not (0)

    % display info
    fprintf('%3i | %5.1f mbar | %5.1f J/g | %5.3f cm³/g | %5.3f g/g\n', i,
p_eq/100, A_eq, W_eq, X_eq)

end

%% write parameter in structure par

par.V_1 = V_1;
par.V_2 = V_2;
par.V_gas = V_gas;
par.m_ac = m_ac;

%% save and rename data structure

save(strcat(folder,'/','dat'), 'dat');
save(strcat(folder,'/','exp'), 'exp');
save(strcat(folder,'/','par'), 'par');

toc
```

Appendix F: MATLAB code

```
%--------------------------Plot Dubinin-Asthakov --------------------------%
clear all;
close all;
tic

%% choose folder

folder = 'GAP_A13_Marina';

% choose color and symbol for isothermal series
symbol = '*';
color  = ['b'; 'g'; 'r'; 'c'; 'y'; 'm'];

fprintf('\nSample: %s\n', folder);

%% load data structures and prepare isothermal data

load([folder,'/','dat.mat']);
load([folder,'/','exp.mat']);
load([folder,'/','par.mat']);


% sort data into isothermal exp series (e.g. 30, 60^\circC)
utiso = unique(exp.T_iso);          % find unique isothermal temps
niso = numel(utiso);

for i=1:exp.n                       % loop over all experiments
    for j=1:niso                    % loop over all temperatures
        if exp.T_iso(i) == utiso(j)
            A_exp(i,j) = exp.A_eq(i);
            W_exp(i,j) = exp.W_eq(i);
        end
    end
end

% save values into iso structure (one entry per isothermal series)
for j=1:niso
   index = find(A_exp(:,j));        % generate index of non-zero entries
   iso(j).A = A_exp(index,j);
   iso(j).W = W_exp(index,j);
   iso(j).T = utiso(j);             % temperature
end

%% generate A and W for DA model

% save DA parameters into vector p
p(1) = par.W_0;
p(2) = par.E;
p(3) = par.n;

A_sim = 0:500;                      % [J/g]
W_sim = Dubinin(p, A_sim);          % [cm^3/g], Dubinin-Asthakov equation
```

Appendix F: MATLAB code

```
%% first plot: DA-model

figure(1)
plot(A_sim, W_sim,'k');
hold on;

% create entries for legend
slegend = cellstr('DA Model');
for j=1:niso
   plot(iso(j).A, iso(j).W, [color(j) symbol])
   slegend(j+1) = { sprintf('Exp %i %cC', iso(j).T, char(176)) };
end
legend('String',slegend);

xlabel('A [J/g]')                % adsorption potential [J/g]
ylabel('W [cm^3/g]')             % capacity [cm^3/g]

saveas(gca, [folder '/plots/' 'DA.pdf']);



%-------------------------Fitting Dubinin-Asthakov-------------------------%

clear all;
close all;
tic

%% choose folder

folder = 'GAP_A13_Marina';

fprintf('\nSample: %s\n', folder);


%% constants
R = 8.3144621;                   % universal gas constant [J/mol/K]
MW = 32.04/100;                  % molecular weight of methanol [J/kg]

%% load data structures

load([folder,'/','exp.mat']);
load([folder,'/','par.mat']);

%% preparation for parameter fitting

i_fit = find(exp.fit);           % get indices of nonzero entries ('fit')
A_exp = exp.A_eq(i_fit);
W_exp = exp.W_eq(i_fit);

i_nofit = find(~exp.fit);        % get indices of zero entries ('nofit')
A_nofit = exp.A_eq(i_nofit);
W_nofit = exp.W_eq(i_nofit);
```

Appendix F: MATLAB code

```
%% parameter fitting for the Dubinin-Astakhov equation

x_0 = [0.5 200 2];                % starting vector [W_0 E n]
[x,resnorm,residual,exitflag,output]=lsqcurvefit(@Dubinin,x_0,A_exp,W_exp);

% fitted parameters
W_0 = x(1);
E = x(2);
n = x(3);

% write parameter in structure par
par.W_0 = x(1);
par.E = x(2);
par.n = x(3);

%% call up plot function

%plots(A_exp, W_exp, v_temp, folder, X_eq, p_eq, psat_MeOH, par);
A_mod = [1:0.1:500];
W_mod = Dubinin(x,A_mod);

figure(1)

% DA-plot
subplot(2,2,1)
plot(A_exp, W_exp, 'kx', A_mod, W_mod, 'k-')
hold on
if numel(A_nofit)>0
    plot(A_nofit, W_nofit, 'ro')
end
xlabel('A [J/g]')
ylabel('W [cm3/g]')
ylim([0 ceil(10*x(1))/10])
grid on

% DA-plot in logarithmic form
subplot(2,2,2)

% residual / error plot: res over A_exp
subplot(2,2,3)
plot(A_exp, residual, 'kx')
xlabel('A [J/g]')
ylabel('residual (W_{mod} - W_{exp})')
xlim([0 500])
grid on

% parity plot: W_mod over W_exp
subplot(2,2,4)
plot(W_exp, Dubinin(x, A_exp), 'kx', [0 1], [0 1], 'k-')
xlim([0 ceil(10*x(1))/10])
ylim([0 ceil(10*x(1))/10])
xlabel('W {exp} [cm3/g]')
```

Appendix F: MATLAB code

```
ylabel('W_{mod} [cm3/g]')

%% final operations

% tabular output
    fprintf('using %i of %i data points for fitting\n\n', numel(i_fit),
numel(exp.A_eq))

    fprintf('%3s | %5s | %5s | %5s | %6s\n', 'i', 'A_exp', 'W_exp', 'W_mod',
'res')
    fprintf('-----------------------------------------\n')
for i=1:numel(A_exp)
    fprintf('%3i | %5.1f | %5.3f | %5.3f | %+6.2e\n', i, A_exp(i), W_exp(i),
Dubinin(x, A_exp(i)), residual(i))
end

fprintf('\n W_0 = %5.3f\n   E = %6.2f\n   n = %4.2f\n res = %5.3e\n\n', x(1),
x(2), x(3), resnorm)

% save parameters in data structure
fn = strcat(folder,'/par.mat');
save(fn, 'par');

toc
```